

Spatial-temporal recurrent reinforcement learning for autonomous ships

Martin Waltz^{a,*}, Ostap Okhrin^{a,b}

^a*Technische Universität Dresden, Chair of Econometrics and Statistics, esp. in the Transport Sector, Dresden, 01062, Germany*

^b*Center for Scalable Data Analytics and Artificial Intelligence (ScaDS.AI), Dresden/Leipzig, Germany*

Abstract

This paper proposes a spatial-temporal recurrent neural network architecture for deep Q -networks that can be used to steer an autonomous ship. The network design makes it possible to handle an arbitrary number of surrounding target ships while offering robustness to partial observability. Furthermore, a state-of-the-art collision risk metric is proposed to enable an easier assessment of different situations by the agent. The COLREG rules of maritime traffic are explicitly considered in the design of the reward function. The final policy is validated on a custom set of newly created single-ship encounters called ‘Around the Clock’ problems and the commonly used Imazu (1987) problems, which include 18 multi-ship scenarios. Performance comparisons with artificial potential field and velocity obstacle methods demonstrate the potential of the proposed approach for maritime path planning. Furthermore, the new architecture exhibits robustness when it is deployed in multi-agent scenarios and it is compatible with other deep reinforcement learning algorithms, including actor-critic frameworks.

Keywords: deep reinforcement learning, recurrency, autonomous surface vehicle, COLREG

*Corresponding author

Email address: `martin.waltz@tu-dresden.de` (Martin Waltz)

1. Introduction

The safety-critical traffic domain can greatly benefit from the use of reliable, autonomously controlled ships. Despite efforts to improve safety measures, human error continues to be the primary cause of maritime accidents. The Annual Overview of Marine Casualties and Incidents 2021 by the European Maritime Safety Agency (2021) revealed that over 53% of maritime accidents between 2014 and 2020 were caused by human actions. This highlights the potential for autonomous surface vehicles (ASVs) to significantly reduce accident rates in maritime operations while also improving the energy and time efficiency, extending operational reliability and precision, and increasing flexibility for dangerous missions (Liu et al., 2016). As a result, there has been a surge of interest, both academic and industrial, in designing ASVs, with projects such as Rolls-Royce (2015), Autoship (2023), and Kongsberg (2023) being carried out alongside studies like those of Johansen et al. (2016), Lyu and Yin (2018), Cheng and Zhang (2018), Zhao and Roh (2019), and Hart et al. (2022).

A crucial characteristic of an ASV is the ability to reliably plan and follow a path toward a specified goal position. The own ship (OS), which is the controlled ASV, should thereby perform collision avoidance (COLAV) with surrounding vessels, called target ships (TSs). Path planning is a well-established field that originated from robotics (see Siciliano et al., 2008, Chapter 7) and there exists a plethora of algorithms developed for this purpose. The most prominent approaches include the artificial potential field (APF) method (Khatib, 1985), velocity obstacles (VO) (Fiorini and Shiller, 1998), genetic algorithms (Holland, 1992), and sampling-based algorithms (Kuffner and LaValle, 2000). We review these approaches in more detail in Section 2. It is important to note that in addition to the inherent limitations of existing algorithms, the *Convention on the International Regulations for Preventing Collisions at Sea* (COLREG) is often overlooked. This convention is a set of rules established by the International Maritime Organization (1972) to enhance maritime traffic safety by defining the proper behaviour for seafarers in certain encounter situations. All vessels in high seas or connected navigable waters must comply with the COLREG rules, making it imperative that any practical path-planning algorithm takes them into account. However, current industry-standard autopilots cannot handle the complex requirements of high-level path-planning and COLREG-compliant COLAV. In fact, according to Heiberg et al. (2022), developing a dynamics model and

control law that can simultaneously perform path following and COLREG-compliant COLAV is an infeasible task for traditional control methods.

In order to overcome these limitations, there have been recent proposals to apply the latest advancements in reinforcement learning (RL; Sutton and Barto, 2018) to the domain of maritime operations. RL is a subfield of artificial intelligence in which an agent, such as a controlled vessel in this case, learns to maximise a reward signal through trial-and-error interaction with its environment. Silver et al. (2021) even hypothesised that any form of intelligence and its associated capabilities can be thought of as maximising a reward signal. Crucially, RL relies on approximations to solve multistage decision problems that could be solved with dynamic programming but have a computationally intractable solution. Hence, some authors refer to RL as *approximate dynamic programming*, and the field has a strong relationship with control theory (Bertsekas, 2019). Recent contributions leveraging the relationship between RL and control theory include those of Vrabie et al. (2009), who proposed an adaptive optimal control method for continuous-time linear systems based on policy iteration, and Xin et al. (2022), who outlined an online RL algorithm for solving multiplayer non-zero sum games.

In recent years, RL has been combined with deep learning (DL; LeCun et al., 2015), which uses neural networks to approximate arbitrary functions with high accuracy (Matsuo et al., 2022). This intersection of RL and DL is known as deep reinforcement learning (DRL), which has achieved remarkable performance in various applications, including complex strategy games (Vinyals et al., 2019), molecule optimisation (Zhou et al., 2019b), advanced racing simulations (Wurman et al., 2022), and even the autonomous navigation of stratospheric balloons over the Pacific Ocean (Bellemare et al., 2020). The methodological basis of these works is often the deep Q -network (DQN) of Mnih et al. (2015), which pairs the off-policy Q -learning algorithm of Watkins and Dayan (1992) with deep neural networks and paved the way for the recent success of DRL. Numerous modifications of the DQN have since been proposed by researchers such as Van Hasselt et al. (2016), Hessel et al. (2018), D’Eramo et al. (2021), and Waltz and Okhrin (2022).

There have been several proposals for DRL in the field of ASVs. For instance, Cheng and Zhang (2018) presented a concise DRL algorithm for obstacle avoidance based on a DQN, although their study only considered static obstacles. Xu et al. (2022a) modified the deep deterministic policy gradient (DDPG) algorithm of Lillicrap et al. (2015) to construct an autonomous COLAV algorithm that considered COLREGs. Nonetheless, their

study only tested relatively simple scenarios. The DDPG algorithm, which is similar to the DQN but was designed for continuous action spaces, was also used by Zhou et al. (2022) to develop an ASV obstacle avoidance method, but traffic rules were not explicitly considered. Sawada et al. (2021) implemented an automatic COLAV system based on the on-policy proximal policy optimisation algorithm (Schulman et al., 2017). The authors explicitly provided predictions of future vessel collisions via the obstacle zone target. Li et al. (2021) combined the DQN with the conventional APF method to design a COLAV algorithm. However, their neural network directly provides a heading change for the OS; therefore, the low-level control routine is not considered part of the DRL task. Fan et al. (2022) constructed a DRL-based maritime COLAV algorithm based on the dueling DQN (Wang et al., 2016), although the validation again considered only simple scenarios with at most two target ships. Other notable contributions include the works of Shen et al. (2019), Guo et al. (2020), Xu et al. (2020), Meyer et al. (2020), Chun et al. (2021), and Xu et al. (2022b) on intelligent ASV control and COLAV using DRL.

All the studies above have in common that the OS must aggregate the information of surrounding target ships to assess the collision risk of a situation and ultimately select an action. The TS information is delivered by the automatic identification system (AIS), which is mandatory equipment for vessels of specific sizes (Lin and Huang, 2006). It can be considered a feature vector for each TS that contains information such as the position, course, and speed. On this basis, two critical challenges arise.

The first challenge is that the number of target ships can vary, making it difficult to process the input vectors with a fully connected neural network with a fixed input size. To address this challenge, various simplifying assumptions and practices have been used in the literature. For instance, Chun et al. (2021) and Xu et al. (2022a) considered only the target ship with the highest collision risk while ignoring all other information, which is not practical since multi-ship encounters require the consideration of multiple vessels. Other researchers such as Xu et al. (2020) attempted to fix a certain number of target ships and train an extra agent for each configuration, which is also not practical since a different control policy is required for each possible number of ships. Zhao and Roh (2019) clustered the input based on possible COLREG encounter situations (see subsection 3.2), but this approach has limitations when multiple target ships are in the same situation. Alternatively, some studies use different observation formats such as

LiDAR beams (Li et al., 2021; Zhou et al., 2022; Meyer et al., 2020) or visual grid input (Woo and Kim, 2020; Sawada et al., 2021), without utilising the available AIS data.

The second challenge in processing AIS data for COLAV is the creation of a robust framework under partial observability, considering that the received data may include delays, noise, and weather-based disturbances (Almalioglu et al., 2022). AIS data may not have a high enough frequency to generate sufficient situational awareness in crowded areas (Heiberg et al., 2022), which suggests the need for the algorithm to process information from several time steps instead of solely relying on the current observation. This approach can improve the ability of the algorithm to handle complex and dynamic situations, reducing the impact of noise and disturbances.

In this paper, we leverage the potential of DRL by designing a simulation-based ASV agent that tackles both challenges. Our contributions to the literature are as follows:

- A *spatial-temporal recurrent* neural network architecture for the DQN is proposed. The approach extends the prior work of Everett et al. (2018, 2021) from the robotic domain and makes it possible to process information in multi-ship encounter situations with a variable number of target ships. Due to the integration of the temporal recurrent component, we achieve robustness against partial observability. Furthermore, our approach offers a fast computational time and makes real-life implementation feasible.
- A *novel collision risk metric* based on the concept of the closest point of approach (CPA; Lenart, 1983) and the ship domain (Goodwin, 1975) is designed. Through the neural architecture and the collision risk metric, we avoid the common hierarchical decomposition of the agent into different sub-controllers, as, for example, in Johansen et al. (2016) and Zhai et al. (2022). Thus, we provide a robust end-to-end solution from AIS data to rudder angle control in maritime operations.
- A suitable training environment with a COLREG-dependent spawning routine of target ships is designed. Additionally, we create *Around the Clock* problems as a comprehensive test-bed for single-ship encounters. Furthermore, our agent is thoroughly validated in multi-encounter scenarios using the *Imazu problems* (Sawada et al., 2021) and two multi-agent situations called the *Star problems*, which are inspired by Zhao

and Roh (2019).

- We compare our approach to two *competitive benchmarks* in the form of the APF method of Huang et al. (2019) and the VO algorithm of Kuwata et al. (2014). In all cases, our agent successfully reaches a specified destination, safely avoids collisions with other vessels, obeys maritime traffic rules, and performs realistic steering actions. These findings highlight the potential of DRL as a promising alternative to traditional algorithmic approaches in the domain of ASV control.

This paper is structured as follows: Section 2 provides maritime background information and further references. Section 3 introduces the modelling of maritime traffic, including the environmental dynamics model, details concerning the COLREGs, and the new collision risk metric. Section 4 presents the RL methodology, outlines the proposed neural network architecture, and describes the state, action, and reward configuration. Section 5 discusses the simulation environment used for training, while the validation scenarios are shown in Section 6. Section 7 concludes this paper. We have made the source code for this paper publicly available at https://github.com/MarWaltz/TUD_RL to enable full reproducibility.

2. Maritime background

2.1. Guidance, navigation, and control

Vagale et al. (2021b) defined ASVs as vessels that have the ability to operate independently without human guidance, navigation, and control (GNC). However, developing such a system is a complex task that requires the consideration of numerous aspects. At the core of an ASV is the navigation module, which estimates the vessel’s current state based on various sensors such as inertial measurement units, global positioning systems, cameras, LiDAR sensors, or RADAR sensors (Liu et al., 2016). Moreover, AIS messages from surrounding target ships can be processed. Using the navigation module’s output, the guidance module of the GNC framework is responsible for generating a reliable geometric path in the form of a set of waypoints that the vessel needs to follow. The ASV system should take into account restrictions on the waterway, assess the collision risk, and perform COLAV with other vessels during this phase. Finally, the control module determines the necessary control forces required to follow the path set by the guidance system.

Path following is traditionally achieved using methods such as line-of-sight (LOS) (Fossen, 2021) or vector field guidance (Nelson et al., 2007) to generate a course command, which is then translated into a low-level control command using traditional approaches such as a proportional-integral-derivative controller. Recently, more advanced learning-based or control-theoretic approaches have also been considered for the latter step (Liu et al., 2018; Woo et al., 2019; Sandeepkumar et al., 2022; Paulig and Okhrin, 2023).

2.2. Practical challenges

Fully autonomous ships present a range of practical challenges that need to be addressed. First, environmental disturbances such as winds, waves, or currents can significantly impact the manoeuvrability of the controlled vessel (Fossen, 2021; Almalioglu et al., 2022) and may affect how vessels behave in encountered situations (Zhou et al., 2019a). Additionally, controlling real ASV systems requires uncertainties resulting from unmodelled dynamics, underactuation, and faults in sensors, actuators, or communication links to be addressed (Liu et al., 2016). Fault diagnosis is a crucial research area that is essential for ensuring the reliable operation of real-life systems (Gao et al., 2015; Tao et al., 2023). Furthermore, the reliable transfer of learning algorithms from simulations to real-world scenarios is still an open research area, with current approaches being heavily dependent on the quality of the simulator (Ju et al., 2022). While approaches such as domain randomisation or domain adaptation may help bridge the sim-to-real gap (Zhao et al., 2020), the maritime domain, with its various sources of disturbances, represents a challenging area for such methods. Finally, unexpected behaviour and the non-cooperation of other ships may arise in practical situations, and cybersecurity threats must also be taken into account (Akdağ et al., 2022). For a more in-depth discussion of these practical issues, we refer readers to Liu et al. (2016) and Akdağ et al. (2022).

2.3. Path planning and collision avoidance

While path following is mostly based on the minimisation of a cross-track or course error, the path-planning task involves strategic decision-making and includes COLAV with target ships. While some papers use a more detailed classification (Breivik et al., 2017; Eriksen et al., 2020), the maritime literature generally distinguishes between two types of path planning: *global* and *local*. Although some algorithms can perform overlapping tasks (Vagale et al., 2021b), global path planning focuses on finding a path from an initial

state to a goal state while accounting for known obstacles. On the other hand, local path planning is reactive and aims to produce a safe and COLREG-compliant path based on online information, thereby enabling COLAV. The focus of this paper is on local path planning. In addition to the DRL-based algorithms outlined in the introduction, there are various conventional approaches for maritime path planning and COLAV, which we review in the following.

A popular planning algorithm is the *artificial potential field* (APF) method, which was first introduced by Khatib (1985) and has since been adapted for the maritime domain (Lyu and Yin, 2018, 2019; Liu et al., 2023). The APF method defines an attractive field for the goal and repulsive fields for obstacles. By superimposing the resulting forces, the vessel is pushed towards the goal while avoiding collisions with other ships. The APF method requires a low computational effort and allows an efficient implementation in practice, but it has the known disadvantages of potentially trapping the vessel in local optima and making goals unreachable when obstacles are nearby (Ge and Cui, 2000).

Velocity obstacles (VO) represent another approach, which was first proposed by Fiorini and Shiller (1998) and successfully adapted for the maritime domain by Kuwata et al. (2014). Instead of considering dynamically moving objects in a positional space, the VO method statically considers the space of velocities of nearby vessels. Based on this, the algorithm computes a velocity obstacle, which is a set of velocities that would lead to a collision in the future under the assumption of the linear movement of another vessel. Recently, non-linear and probabilistic trajectories have also been considered (Huang et al., 2018, 2019). After computing the VO for each vessel, the algorithm selects a velocity vector that does not lie in the union of the VO sets. The selection is performed via the optimisation of some objective, such as the deviation from a desired velocity. The disadvantage of VO approaches is that the solution space may be empty (Ribeiro et al., 2021), or the vessel may exhibit undesired oscillatory motions (Tang et al., 2023).

Genetic algorithms (GAs) represent another widely used option for optimisation and particularly planning problems (Holland, 1992; Öztürk et al., 2022). GAs use principles inspired by biological evolution, such as reproduction, mutation, and selection, to find the optimal solution to a problem. For instance, Kim et al. (2017) outlined an approach for autonomous maritime path planning based on a GA while specifying avoiding obstacles, reaching a target point, and minimising the travel time as the objective func-

tions. Further recent marine GA contributions include those of Ning et al. (2020) and Wang et al. (2021). Although GAs have the potential to generate collision-free paths, they suffer from significant computation times, making them challenging to deploy in practice (Tam and Bucknall, 2010).

Sampling-based algorithms like *rapidly exploring random trees* (RRTs) represent more approaches from the robotics domain and are particularly useful for high-dimensional spaces and non-linear systems, where other methods can struggle (Kuffner and LaValle, 2000; LaValle and Kuffner Jr, 2001). The basic idea behind RRTs is to build a tree structure that explores the search space in a randomised way, gradually expanding to cover more and more of the space. Karaman and Frazzoli (2011) provided a detailed analysis and proposed several competitive modifications of the original RRT algorithm. Chiang and Tapia (2018), Zaccone et al. (2019), and Enevoldsen et al. (2021) proposed different adaptations of RRT-based algorithms to the maritime domain that consider traffic rules. Sampling-based approaches have some primary drawbacks, including their potentially long computation times and their dependence on a forward simulator to predict the behaviour of target ships (Chiang and Tapia, 2018).

Model predictive control (MPC) algorithms are a powerful class of algorithms that can be used for path planning. MPC algorithms can compute optimal trajectories using an environmental model that describes the surrounding environment in detail (Garcia et al., 1989). During optimisation, MPC can consider several factors that affect the trajectory, including nonlinear dynamics, constraints, and disturbances. Johansen et al. (2016) proposed an MPC-based planner that controls the speed and course of a vessel while using LOS guidance and a proportional-integral controller to translate the course command into a rudder angle. Further maritime applications of MPC include those of Abdelaal et al. (2018), Hagen et al. (2018), and Wang et al. (2020). The main limitations of MPC-based proposals when it comes to practical applications are possible convergence issues and the computational complexity (Hagen et al., 2018).

This list of methods is far from being complete; in addition, there are several other algorithms for maritime path planning and COLAV, such as dynamic-window approaches (Serigstad et al., 2018), ant colony optimisation (Lazarowska, 2015), and fast marching methods (Liu and Bucknall, 2015). For further reading on this topic, we recommend the reviews provided by Vagale et al. (2021a), Zhai et al. (2022), and Öztürk et al. (2022). As mentioned above, those techniques are mainly used for path planning and rely

on a separate module for path following that involves the low-level control of actuators. This contrasts with our DRL approach, which provides an end-to-end solution, tackling local path planning and following simultaneously.

3. Modelling of maritime traffic

3.1. Environmental dynamics

We consider the Manoeuvring Modelling Group (MMG) model of Yasukawa and Yoshimura (2015) to describe the dynamics of the full-scale KVLCC2 (Stern et al., 2011) tanker. Several related works (Cheng and Zhang, 2018; Heiberg et al., 2022; Du et al., 2022) instead rely on the miniature model ship CyberShip II, with the hydrodynamic parameters identified by Skjetne et al. (2004). However, we have chosen the KVLCC2 since it has a length between perpendiculars of $L_{pp} = 320$ m, allowing for a more realistic setup on the ocean, and the corresponding dynamics model was identified and extensively tested by Yasukawa and Yoshimura (2015). Our simulation relies on the following assumptions, which are frequently imposed when maritime traffic is modelled (Meyer et al., 2020; Heiberg et al., 2022):

Assumption 1: Calm sea. *There are no external disturbances in the form of wind, waves, or currents.*

Assumption 2: Motion restriction. *The vessel is located on a horizontal plane with no heave, pitch, and rolling motion.*

Consequently, the model consists of 3 degrees of freedom, and the navigational state of the vessel is described by $\eta = (x_n, y_n, \psi)^\top$. The elements x_n and y_n are the north and east coordinates relative to a coordinate origin o_n in the *North-East-Down* system $\{n\}$, where ψ is the vessel’s heading and is defined as the angle between the x_n -axis and the x_b -axis of the *body-fixed* reference frame $\{b\}$, which is centred at the midship position. In $\{b\}$, x_b corresponds to the longitudinal axis, while y_b is the transversal (starboard) axis. The velocity of the vessel is described by $\nu = (u, v, \tilde{r})^\top$, where u and v are the components in the x_b and y_b directions, respectively, and \tilde{r} is the yaw rate. Furthermore, we define the drift angle $\beta = \arctan(v/u)$, the total speed $U = \sqrt{u^2 + v^2}$, and the course angle $\chi = \psi + \beta$ (Fossen, 2021). Figure 1 illustrates the coordinate systems. The following set of equations connects

$\{n\}$ and $\{b\}$ via rotation:

$$\begin{aligned}\dot{x}_n &= u \cos \psi - v \sin \psi, \\ \dot{y}_n &= u \sin \psi + v \cos \psi, \\ \dot{\psi} &= \tilde{r},\end{aligned}\tag{1}$$

where \dot{w} denotes the (later component-wise) first-order derivative of w . The equations of motion governing the dynamics of the vessel are

$$\begin{aligned}(m + m_{x_b})\dot{u} - (m + m_{y_b})v\tilde{r} - x_G m \tilde{r}^2 &= X = X_H + X_R + X_P, \\ (m + m_{y_b})\dot{v} + (m + m_{x_b})u\tilde{r} + x_G m \dot{\tilde{r}} &= Y = Y_H + Y_R, \\ (I_{z_G} + x_G^2 m + J_z)\dot{\tilde{r}} + x_G m(\dot{v} + u\tilde{r}) &= N_m = N_H + N_R,\end{aligned}\tag{2}$$

where m is the ship's mass, m_{x_b} and m_{y_b} are the added masses in the x_b and y_b directions, respectively, x_G is the longitudinal coordinate in $\{b\}$ of the centre of gravity (COG) of the ship, I_{z_G} is the moment of inertia of the ship around the COG, and J_z is the added moment of inertia. Furthermore, X is the surge force, Y is the lateral force, and N_m is the yaw moment around midship. These forces consist of their respective hull (H), rudder (R), and propeller (P) components. Yasukawa and Yoshimura (2015) provided detailed expressions for each force, along with parameters for the full-scale KVLCC2 tanker, and we refer the reader interested in the fine details to this paper. Crucially, by adjusting the tanker's rudder angle δ , we can control the related rudder forces X_R , Y_R , and N_R and realise steering commands.

We use a subscript t to refer to a particular quantity at time t , e.g. η_t and ν_t refer to the navigation and velocity vectors, respectively. We discretise the dynamics using a step size of 3 s, and thus η_{t+1} corresponds to 3 s in real time after η_t . To obtain η_{t+1} and ν_{t+1} , we solve the systems of equations (1) and (2) for the derivatives $\dot{\eta}_t$ and $\dot{\nu}_t$, and we use the ballistic method of Treiber and Kanagaraj (2015). The latter consists of an Euler update for the speeds and a trapezoidal update for the positions.

3.2. International Regulations for Preventing Collisions at Sea

3.2.1. Overview

Compliance with the COLREG rules of the International Maritime Organization (1972) is mandatory for vessels operating in high seas. However, the 41 rules lack specific, measurable quantities that can be used to determine

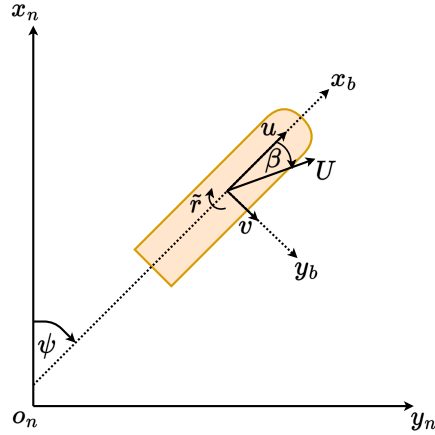


Figure 1: Visualisation of the coordinate systems $\{n\}$ and $\{b\}$, similar to Yasukawa and Yoshimura (2015).

whether a particular behaviour was COLREG-compliant or not. Notably, in the 1970s, when the rules were published, there were no autonomous vessel systems, and the regulations were tailored to human seafarers and decision-makers. As pointed out by Heiberg et al. (2022), modern optimisation approaches do not necessarily produce COLREG-compliant actions. For example, COLAV actions must be substantial and visible to make the agent’s intentions transparent to other traffic participants. However, such behaviour mostly does not result in fuel or time efficiency. The combination of autonomous and human-controlled vessels and potential changes to the regulatory rule set constitute an active area of research (Zhou et al., 2020; Miyoshi et al., 2022).

For the reader’s convenience, Appendix A contains concrete passages of the rules that are especially relevant for maritime traffic modelling. To briefly summarise the most important COLREGs, each vessel should proceed at a safe speed to effectively avoid collisions, determine if the risk of collision exists, and take substantial COLAV actions to pass other vessels at a safe distance. Moreover, the COLREGs categorise vessels into give-way and stand-on vessels, depending on their role in one of four possible encounter situations (see Figure 2). Generally, give-way vessels are required to keep out of the other vessel’s way, while stand-on vessels should keep their current course and speed. For example, both vessels are classified as give-way in a head-on scenario (Figure 2, Panel A) and should change their course to starboard.

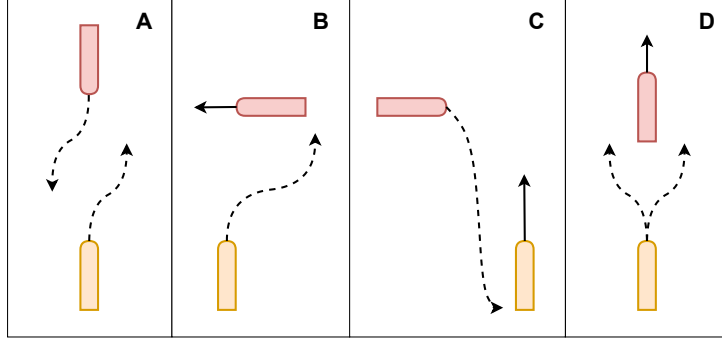


Figure 2: Visualisation of the COLREG encounter situations based on Vagale et al. (2021b). The OS is yellow and the TS is red. There are four scenarios: (A) head-on, (B) starboard crossing, (C) port crossing, and (D) overtaking. The give-way vessel is depicted with a dashed line, while the stand-on vessel is depicted with a solid line.

Similar to Woo and Kim (2020) and Xu et al. (2022b), we will assume that the target ships move linearly and deterministically in our simulation. Therefore, our work focuses on cases in which the OS is the give-way ship and is responsible for actively avoiding collisions. Subsection 3.2.2 discusses the criteria for each encounter scenario.

3.2.2. Scenario classification

Whether a scenario at sea is classified as one of the four encounter situations depends on the two vessels' angular and positional constellation, which is measured using two quantities (see Figure 3). The first is the heading intersection angle $C_T = [\psi_{TS} - \psi_{OS}]_0^{2\pi}$, where ψ_{TS} and ψ_{OS} are the headings of the TS and the OS, respectively, with the clipping operation to $[a, a + 2\pi)$ for $a \in \{-\pi, 0\}$ defined as $[\cdot]_a^{a+2\pi}$:

$$[\theta]_a^{a+2\pi} = \begin{cases} \theta - \lfloor \frac{\theta-a}{2\pi} \rfloor \cdot 2\pi & \text{if } \theta \geq 0, \\ \theta + (\lfloor \frac{-\theta-a}{2\pi} \rfloor + 1) \cdot 2\pi & \text{if } \theta < 0, \end{cases}$$

where the floor operator, which returns the largest integer smaller than the argument, is denoted by $\lfloor \cdot \rfloor$ (Benjamin, 2017).

Second, α_{OS}^{TS} , the relative bearing from the OS to the TS, is computed as the difference between the absolute bearing, β_{OS}^{TS} , and the OS's heading: $\alpha_{OS}^{TS} = [\beta_{OS}^{TS} - \psi_{OS}]_0^{2\pi}$. Conversely, α_{TS}^{OS} and β_{TS}^{OS} are the quantities from the perspective of the TS toward the OS. Scenarios can be classified based on the heading intersection angle and the relative bearing, as outlined in Table

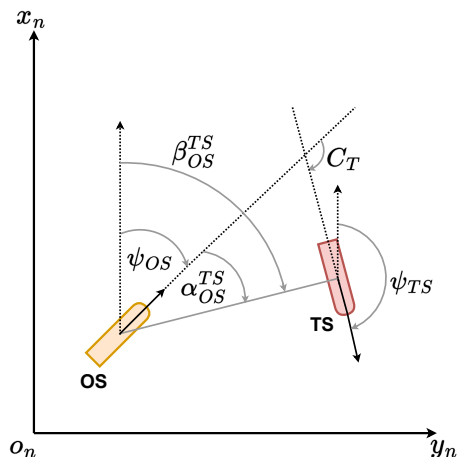


Figure 3: Visualisation of the heading intersection angle C_T , the relative bearing α_{OS}^{TS} , and the absolute bearing β_{OS}^{TS} .

1, and they are visualised in Figure 2. Note that the rules should always be seen in the context of the present situation at sea, and seafarers consider softly defined practices referred to as good seamanship.

Moreover, the definitions above focus solely on situations with two vessels. In practice, multi-ship situations are possible, especially in highly congested sea areas. A reliable control system needs to effectively process the information of all relevant target ships to find a safe path in these cases, despite the insufficiently defined rule set (Kang et al., 2021).

3.3. Collision risk assessment

3.3.1. Ship domain and CPA

Assessing the collision risk with other vessels is required by the COLREGs and constitutes a fundamental part of an ASV. The methodological repertoire of the literature is diverse and has recently been reviewed by Öztürk and Cicek (2019) and Huang et al. (2020). Two crucial approaches are the definition of ship domains (Goodwin, 1975; Śmierczalski, 2005; Szlapczynski and Szlapczynska, 2017) and the concept of the closest point of approach (Mou et al., 2010; Zhao and Roh, 2019). The ship domain is a safe area around the vessel, which should not be entered by other ships. Several geometric representations of ship domains have been considered, and they are primarily asymmetric, with a larger space on the starboard side to enable

Situation	σ	Requirements	Action from OS
Head-on	1	$\alpha_{OS}^{TS} \in \{[0^\circ, 5^\circ] \cup [355^\circ, 360^\circ]\}$ $C_T \in [175^\circ, 185^\circ]$	Alter course to starboard, pass TS on its portside
Starboard crossing	2	$\alpha_{OS}^{TS} \in [5^\circ, 112.5^\circ]$ $C_T \in [185^\circ, 292.5^\circ]$	Alter course to starboard, avoid crossing ahead of TS
Port crossing	3	$\alpha_{OS}^{TS} \in [247.5^\circ, 355^\circ]$ $C_T \in [67.5^\circ, 175^\circ]$	Keep course, TS is give-way vessel
Overtaking	4	$\alpha_{TS}^{OS} \in [112.5^\circ, 247.5^\circ]$ $C_T \in \{[0^\circ, 67.5^\circ] \cup [292.5^\circ, 360^\circ]\}$ $U_{OS,R} > U_{TS}$	Overtake on any side, keep out of TS's way

Table 1: Classification of COLREG encounter situations between two vessels following Xu et al. (2020). We define the variable σ to refer to a particular scenario. If no requirements are fulfilled, we set $\sigma = 0$. Overtaking imposes, in addition to C_T and α_{OS}^{TS} , a third constraint, namely that the relative speed of the OS in the direction of the TS's course, $U_{OS,R}$, is larger than the TS's total speed U_{TS} .

COLREG-compliant COLAV. While there are several possibilities for defining a collision based on the ship domain (Heiberg et al., 2022), in this study, we define the TS's midship position being at or inside the OS's ship domain as a collision event. While the non-violation of the ship domain equates to reliable COLAV, the approach lacks a quantitative collision risk metric since the violation or non-violation of the domain is a binary variable (Ha et al., 2021).

Filling this gap, the CPA concept describes the closest point two vessels will encounter under the assumption that both keep their course and speed. Two key quantities are the time until the CPA is reached, called the TCPA, and the distance between the two vessels at the CPA, called the DCPA (Lenart, 1983):

$$\begin{aligned}
\text{TCPA} &= -\frac{(x_{n,TS} - x_{n,OS}) \cdot v_{r,x_n} + (y_{n,TS} - y_{n,OS}) \cdot v_{r,y_n}}{v_{r,x_n}^2 + v_{r,y_n}^2}, \\
\Delta x_{n,\text{TCPA}} &= (x_{n,OS} + \text{TCPA} \cdot v_{x_n,OS}) - (x_{n,TS} + \text{TCPA} \cdot v_{x_n,TS}), \\
\Delta y_{n,\text{TCPA}} &= (y_{n,OS} + \text{TCPA} \cdot v_{y_n,OS}) - (y_{n,TS} + \text{TCPA} \cdot v_{y_n,TS}), \\
\text{DCPA} &= \sqrt{(\Delta x_{n,\text{TCPA}})^2 + (\Delta y_{n,\text{TCPA}})^2},
\end{aligned} \tag{3}$$

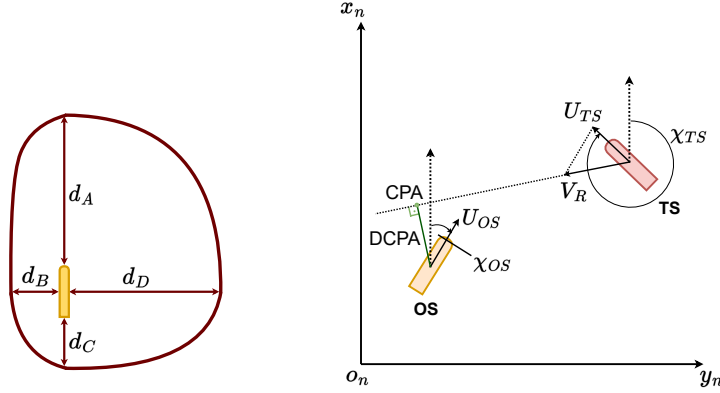


Figure 4: Visualisation of the collision risk assessment methods used in this work. The left-hand side shows the asymmetric ship domain of Chun et al. (2021), which we construct as a combination of four ellipses with $d_A = d_D = 3L_{pp}$ and $d_B = d_C = L_{pp}$. The right-hand side visualises the concepts of the CPA and DCPA based on Heiberg et al. (2022). In this illustration, the heading equals the course angle for both vessels.

where $x_{n,OS}$, $y_{n,OS}$, $v_{x_{n,OS}}$, and $v_{y_{n,OS}}$ are the positions and speeds of the OS in $\{n\}$, respectively. The notation for the TS is similar, and the relative speeds are $v_{r,x_n} = v_{x_{n,TS}} - v_{x_{n,OS}}$ and $v_{r,y_n} = v_{y_{n,TS}} - v_{y_{n,OS}}$. The drawback of the CPA-based metrics is their inability to reliably guarantee COLAV when analysed in isolation (Ha et al., 2021) and the abstraction from present yaw moments and future non-linear behaviour. Figure 4 illustrates these concepts.

3.3.2. Construction of a collision risk metric

The construction of a reliable collision risk metric is of central importance for an RL agent since it directly signals the criticality of an opposing ship. Based on the concepts from subsection 3.3.1, we develop a novel CR metric, unifying the concepts CR_{CPA} and CR_{ED} , which will be defined later, as follows:

$$CR = \begin{cases} 1 & \text{if TS in ship domain of OS,} \\ \max(CR_{CPA}, CR_{ED}) & \text{otherwise.} \end{cases} \quad (4)$$

For all situations, $CR \in [0, 1]$, where 0 suggests no risk of collision and 1 is a collision event. Through the maximum operator, we consider the more critical of the two components CR_{CPA} and CR_{ED} . The first component,

CR_{CPA} , signals a large collision risk if the TCPA (absolute value) and DCPA are small since the OS then faces a potentially dangerous situation in the near future. The second component, CR_{ED} , considers that a small Euclidean distance between two ships indicates a high risk of collision. The necessity of introducing this second component is discussed in detail below.

Building on Mou et al. (2010), we define CR_{CPA} to behave exponentially in negative TCPA and DCPA:

$$CR_{CPA} = \exp \left\{ c_1 \cdot \left[DCPA' + c_2^{\mathbf{1}\{\text{TCPA} \geq 0\}} \cdot c_3^{\mathbf{1}\{\text{TCPA} < 0\}} |\text{TCPA}| \right] \right\}, \quad (5)$$

where we set $c_1 = \log(0.1)/3704$, $c_2 = 1.5$, and $c_3 = 20$ in our simulation. Note that 3704 m is equal to 2 nautical miles (NM) and that the sign of c_1 is negative. The indicator function $\mathbf{1}\{x\}$ is 1 if x is true and 0 otherwise. Since we set $c_2 < c_3$, we weight positive and negative TCPA values differently and achieve a rapid decay in the collision risk after the CPA has been passed while avoiding a jump in the metric by, e.g. setting the CR_{CPA} component to zero. Furthermore, instead of directly using the DCPA value from (3), we consider the distance of the TS to the OS's ship domain via the following modification:

$$DCPA' = f_{DCPA} \cdot \max \left[0, DCPA - D(\alpha_{OS,CPA}^{TS}) \right]. \quad (6)$$

The function $D : [0, 2\pi) \rightarrow \mathbb{R}$ returns the distance to the ship domain for a given encounter angle, which is non-constant since we consider an asymmetric shape (see Figure 4). Furthermore, we denote the relative bearing from the perspective of the OS towards the TS at the CPA, or equivalently, at $\text{TCPA} = 0$, with $\alpha_{OS,CPA}^{TS}$. Thus, we consider the safety area of the OS at the CPA. Moreover, we want to explicitly avoid the scenario in which the agent crosses at the bow of other ships, which is considered bad practice at sea. The factor f_{DCPA} is responsible for this:

$$f_{DCPA} = \begin{cases} c_4 - \exp(c_5 \cdot |[\alpha_{TS,CPA}^{OS}]_{-\pi}|) & \text{if } \text{TCPA} \geq 0 \text{ and } |[\alpha_{TS,CPA}^{OS}]_{-\pi}| \leq \frac{\pi}{6}, \\ 1 & \text{otherwise,} \end{cases}$$

where $\alpha_{TS,CPA}^{OS}$ is the relative bearing from the perspective of the TS towards the OS at the CPA, and $c_4 = 1.2$ and $c_5 = -\log(5)/\frac{\pi}{6}$ are constants. This factor penalises the undesired crossing behaviour by decreasing the sensed distance at the CPA and thus increasing the risk of collision. Figure 5 visu-

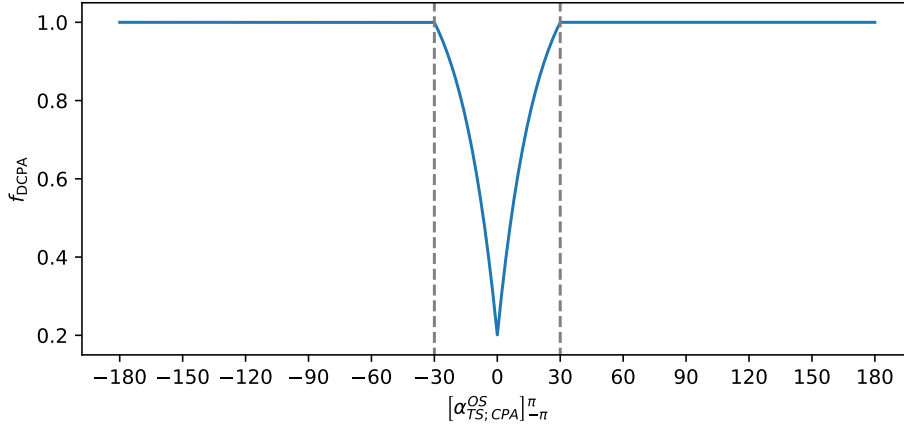


Figure 5: Specification of the factor f_{DCPA} for bow-crossing avoidance. The illustration shows the case in which $\text{TCPA} \geq 0$, and $[\alpha_{\text{TS};\text{CPA}}^{\text{OS}}]_{-\pi}^{\pi}$ is given in degrees.

alises the behaviour of this factor.

The component CR_{CPA} is a reasonable quantification of the collision risk in the majority of scenarios. However, there are distinct disadvantages that made the inclusion of the component CR_{ED} based on the Euclidean distance between the ships, denoted $d_{\text{OS}}^{\text{TS}}$, necessary. Consider a scenario in which two ships are close but have almost the same course. The CPA-based metrics signal that this situation is not risky since the CPA either lies a long time in the past or is far in the future. However, if a ship turns even slightly, the absolute value of the TCPA jumps to a much smaller value, and suddenly the situation is precarious. To prevent this drawback, we define the second component as follows:

$$CR_{\text{ED}} = \exp \left\{ c_6^{-1} \cdot [d_{\text{OS}}^{\text{TS}} - D(\alpha_{\text{OS}}^{\text{TS}})] \right\}, \quad (7)$$

where $c_6 = -0.3 \cdot 3704 = -1111.2$ is a negative constant. The subtraction of the distance to the ship domain is motivated as in (6).

We emphasise that the functional relationships (4)–(7) build a robust collision risk metric for vessels of various classes. However, we set the constants c_1, \dots, c_6 specifically for the KVLCC2 tanker, and these values should be adjusted for a vessel with different characteristics and manoeuvrability. Moreover, similar to how human seafarers have different interpretations of safe passing distances (Miyoshi et al., 2022), the ASV designer can calibrate

c_1, \dots, c_6 depending on how risk-averse the agent should be.

4. Reinforcement learning methodology

4.1. Background

Reinforcement learning is a methodological ensemble in which an agent learns based on trial and error in an environment (Sutton and Barto, 2018). The common formalism of the problem is a Markov decision process (MDP; Puterman, 1994), which is represented by the tuple $(\mathcal{S}, \mathcal{A}, \mathcal{P}, \mathcal{R}, \gamma)$. \mathcal{S} is the state space, \mathcal{A} is the discrete action space, $\mathcal{P} : \mathcal{S} \times \mathcal{A} \times \mathcal{S} \rightarrow [0, 1]$ is the state transition probability distribution, $\mathcal{R} : \mathcal{S} \times \mathcal{A} \rightarrow \mathbb{R}$ is a bounded reward function, and $\gamma \in [0, 1)$ is the discount factor. At each step t , the agent receives state information $s_t \in \mathcal{S}$, takes an action $a_t \in \mathcal{A}$ according to a policy $\pi : \mathcal{S} \times \mathcal{A} \rightarrow [0, 1]$, gets a reward r_t generated by \mathcal{R} , and transitions according to \mathcal{P} to the next state $s_{t+1} \in \mathcal{S}$. Transferred to our maritime application case, the state includes the positional and motion information of the ships, while the action is the change in the rudder angle of the OS.

The discounted sum of rewards during an episode is called the return. Many frequently used RL algorithms define action-values: $Q^\pi(s, a) = \mathbb{E}[\sum_{t=0}^{\infty} \gamma^t r_t | s_0 = s, a_0 = a]$. Thus, these so-called Q -values describe the expected return when action a in state s is executed and policy π is followed afterward. The methodological basis of our work is the Q -learning algorithm of Watkins and Dayan (1992). The objective of the algorithm is to attain the optimal action-values $Q^*(s, a)$ for all $s \in \mathcal{S}, a \in \mathcal{A}$, which yield an optimal policy $\pi^*(s) = \arg \max_{a' \in \mathcal{A}} Q^*(s, a')$ for all $s \in \mathcal{S}, a \in \mathcal{A}$ if such an optimal policy exists; see Puterman (1994) for a deep discussion. The convergence conditions for Q -learning are relatively mild (Tsitsiklis, 1994).

Storing a Q -value for each state-action pair is infeasible for continuous state spaces, which occur in our maritime environment. Mnih et al. (2015) proposed the DQN algorithm, an extension of Q -learning in which action-values are approximated by deep neural networks. More precisely, we consider the function $Q(s, a; \theta)$ for all $s \in \mathcal{S}, a \in \mathcal{A}$, where θ is the parameter set of the neural network. The optimisation is performed using gradient descent:

$$\theta \leftarrow \theta + \tau [y - Q(s, a; \theta)] \nabla_{\theta} Q(s, a; \theta),$$

where $y = r + \gamma \max_{a' \in \mathcal{A}} Q(s', a'; \theta^-)$. The successor state after action a is executed in state s is denoted s' , τ is the learning rate, and θ^- is the

parameter set of the target network, a time-delayed copy of θ . Moreover, the DQN uses experience replay to stabilise the training.

4.2. Spatial-temporal recurrent architecture

In practice, observing the full state of a system is often not possible due to sensor limitations, noise, time delays, and other factors. Acknowledging this circumstance, we formally consider a partially observable MDP (POMDP; Kaelbling et al., 1998), which extends the MDP-tuple $(\mathcal{S}, \mathcal{A}, \mathcal{P}, \mathcal{R}, \gamma)$ of subsection 4.1 by adding two components: the observation space \mathcal{O} and the observation function $\mathcal{Z} : \mathcal{S} \times \mathcal{A} \times \mathcal{O} \rightarrow [0, 1]$. At time t , instead of receiving the full state $s_t \in \mathcal{S}$, the agent receives an observation $o_t \in \mathcal{O}$, which is generated by \mathcal{Z} . On an implementation level, for the DQN, the action-value function receives as input an observation $o \in \mathcal{O}$ instead of the state $s \in \mathcal{S}$.

Recently, Meng et al. (2021) proposed the LSTM-TD3 algorithm, an extension of the TD3 algorithm of Fujimoto et al. (2018), to deal with POMDPs. A memory extraction component based on a long short-term memory (LSTM; Hochreiter and Schmidhuber, 1997) architecture processes several past observations, and it combines this information with the observation of the current time step. Thus, the LSTM-TD3 incorporates a *temporal recurrency*, which allows information from observation sequences over time to be processed.

In our maritime application case, an observation $o_t = o_{OS,t} \cup o_{TS,t}$ consists of two components: $o_{OS,t}$, the information regarding the navigational status of the OS, and $o_{TS,t}$, the information of the surrounding target ships. The observation $o_{TS,t}$ consists of features inspired by AIS data and will be described in detail in subsection 4.3. Importantly, the size of $o_{TS,t}$ is $N_t \cdot 6$, where N_t is the number of the target ships surrounding the OS at time t . Crucially, N_t can change over time; it cannot be processed with a standard fully connected neural network that requires a fixed input size. Building on the work of Everett et al. (2018, 2021), we propose a more flexible approach by introducing a *spatial recurrence* that sequentially processes the target ships according to their estimated collision risk. Similar to the temporal LSTM, which loops over sequences of observations of different time steps, the introduced spatial LSTM loops over the sub-observations of different target ships *at the same point in time*.

In the proposed architecture, we implement both *temporal* and *spatial recurrency* components. Thus, we can deal with an arbitrary number of target ships while efficiently processing information over several time steps.

Formally,

$$\begin{aligned} x_{t-l} &= f_l(o_{OS,t-l}, o_{TS,t-l}; \theta_{f_l}) \quad \text{for } l = 0, \dots, h, \\ Q(o_{(t-h):t}, a_i; \theta) &= g(x_{t-h}, \dots, x_{t-1}, x_t, a_i; \theta_g) \quad \text{for } i = 1, \dots, M, \end{aligned}$$

where M is the cardinality of the action space and $o_{(t-h):t} = \cup_{l=0}^h o_{t-l}$. The number of considered past observations is h , and we fix $h = 2$ throughout the paper since it provides a very good performance. The functions f_l with parameters θ_{f_l} for $l = 0, \dots, h$ represent the spatial recurrency, and the function g , parametrised by θ_g , corresponds to the temporal recurrency. The complete parameter set is $\theta = (\cup_{l=0}^h \theta_{f_l}) \cup \theta_g$ and the architecture is illustrated in Figure 6. The algorithmic procedure is identical to the DQN outlined in Mnih et al. (2015), and the approach is compatible with further modifications like those of Schaul et al. (2015), Van Hasselt et al. (2016), or Waltz and Okhrin (2022). It is worth noting that there are different ways to incorporate temporal recurrence into the architecture. While our method takes advantage of the promising outcomes demonstrated by Meng et al. (2021) by processing the current observation alongside the previous h time steps, other studies directly store and process the entire history of the episode in recurrent layers (Heess et al., 2015; Wang et al., 2019). Although this represents an interesting area for future research, our current approach delivers a robust performance, and we chose to maintain it for the scope of this paper.

4.3. Observation and action spaces

We define $o_{OS,t}$, the OS-related component of the observation at time t , by considering the OS’s velocity information and rudder angle, together with the Euclidean distance $d_{OS,t}^G$ and relative bearing $\alpha_{OS,t}^G$ to the goal $(x_{n,G}, y_{n,G})$:

$$o_{OS,t} = \left(\frac{u_t}{u_{\text{scale}}}, \frac{v_t}{v_{\text{scale}}}, \frac{\tilde{r}_t}{\tilde{r}_{\text{scale}}}, \frac{\dot{\tilde{r}}_t}{\dot{\tilde{r}}_{\text{scale}}}, \frac{\delta_t}{\delta_{\text{scale}}}, \frac{d_{OS,t}^G}{d_{\text{scale}}}, \frac{[\alpha_{OS,t}^G]_{-\pi}^{\pi}}{\pi} \right)^\top.$$

The denominators are scaling factors: $u_{\text{scale}} = 7 \text{ m/s}$, $v_{\text{scale}} = 0.7 \text{ m/s}$, $\tilde{r}_{\text{scale}} = 0.004 \text{ rad/s}$, $\dot{\tilde{r}}_{\text{scale}} = 8 \cdot 10^{-5} \text{ rad/s}^2$, $\delta_{\text{scale}} = 20^\circ$, and $d_{\text{scale}} = 14 \text{ NM}$ to achieve inputs approximately in the interval $[-1, 1]$. To define $o_{TS,t}$, the feature vector of the target ships at time t , we assume that we have access to the AIS data of other ships to obtain their course, speed, and positional information, which serve as the input to our deep Q -network. Precisely, the component is

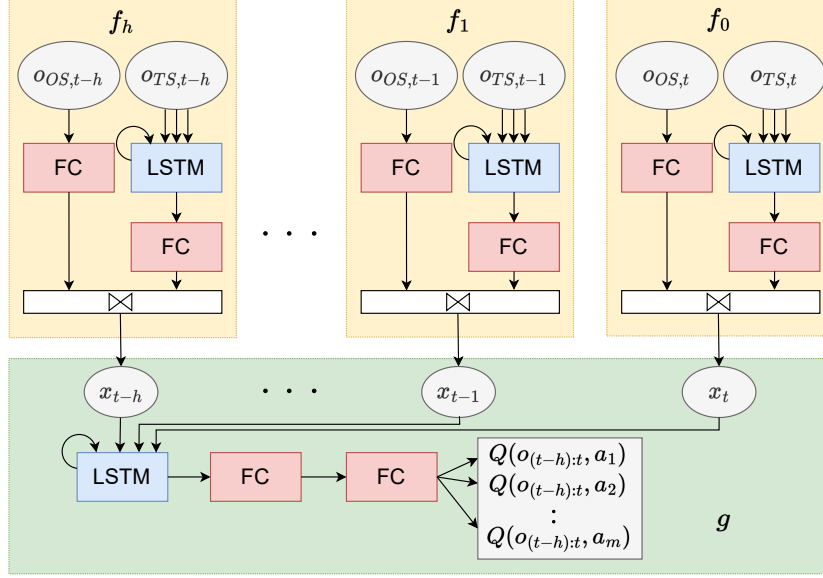


Figure 6: Spatial-temporal recurrent architecture. The concatenation symbol is \otimes , and FC refers to a fully connected layer with 64 output features, as specified in deep learning frameworks like PyTorch (Paszke et al., 2019). Thus, strictly speaking, it is one weight matrix rather than a layer. We use ReLU activations after each FC block except for the last one, which applies the identity function to yield Q -value estimates in \mathbb{R}^M . The number of hidden units in the LSTM blocks is 64.

defined as follows:

$$o_{TS,t} = (o_{1,t}, \dots, o_{N_t,t})^\top,$$

where $o_{i,t}$, with $i = 1, \dots, N_t$, is the information about the i th target ship at time t ; the $o_{i,t}$ vectors are sorted with respect to *ascending collision risk*, following the newly defined metric in subsection 3.3.2. Again, the size of $o_{TS,t}$ depends on N_t . The feature vector for TS i is defined as

$$o_{i,t} = \left(\frac{[C_{T,i,t}]^\pi}{\pi}, \frac{U_{i,t}}{u_{\text{scale}}}, \frac{d_{OS,t}^i - D(\alpha_{OS,t}^i)}{d_{\text{scale}}}, \frac{[\alpha_{OS,t}^i]^\pi}{\pi}, \sigma_{i,t}, CR_{i,t} \right)^\top,$$

where $\sigma_{i,t}$ is the COLREG-encounter situation from Table 1. The element $CR_{i,t}$ is our collision risk metric for ship i at time t . Crucially, if no target ship is present, our recurrent structure still requires information about at least one ship. In this case, we artificially create a no-risk target ship $o_{TS,t} = o_{1,t} = (-1, 0, 1, -1, 0, 0)^\top$. This technical padding procedure is unavoidable

when dealing with neural networks. However, due to our recursive structure, we need to pad information about one ship maximally instead of padding the whole surrounding area, as is the case when specifying a non-recursive architecture.

Regarding the action space, the agent can only control changes in the rudder angle by selecting one of three actions: $a_t \in \{0, -\Delta\delta, \Delta\delta\}$. We set $\Delta\delta = 5^\circ$ in our simulation, which builds, together with our simulation step size of 3 s, a realistic steering behaviour of $\sim 1.67^\circ/\text{s}$. Furthermore, we clip the rudder angle to an absolute value of 20° . We do not allow thrust control to keep the action space as simple as possible, and, in practice, steering is generally preferred over thrust changes, especially for a large tanker like the KVLCC2. Thus, we keep the revolutions per second of the propeller fixed to 1.8 for the OS, which results in a speed of $\sim 7.42 \text{ m/s}$ without steering.

4.4. Reward design

The reward function plays a crucial role in RL applications, as it is used to obtain the desired behaviour of the agent. While we aimed to keep the reward function as simple as possible, we identified five key components that were necessary for developing a robust end-to-end agent that could generate appropriate rudder angles from AIS data. These components are a heading and distance reward towards the goal, a collision penalty, a traffic rule component, and a comfort reward. We must admit that many parameters were experimentally obtained in order to obtain the best performance.

Building on the work of Xu et al. (2022a), the heading and distance reward enables the agent to construct a path towards the goal:

$$r_{\text{dist},t} = \frac{d_{\text{OS},t-1}^{\text{G}} - d_{\text{OS},t}^{\text{G}}}{c_7} + c_8, \quad r_{\text{head},t} = -\frac{|[\alpha_{\text{OS},t}^{\text{G}}]_{-\pi}|}{\pi},$$

with constants $c_7 = 20$ and $c_8 = -1$. Note that the speed of the OS is constant at $\sim 7.42 \text{ m/s}$ and that our simulation step size is 3 s. Thus, if the OS is moving straight toward the goal, we have $d_{\text{OS},t-1}^{\text{G}} - d_{\text{OS},t}^{\text{G}} \approx 3 \text{ s} \cdot 7.42 \text{ m/s} = 22.26 \text{ m}$. Consequently, with the given values of c_7 and c_8 , the distance reward is in $[-2.113, 0.113]$, while the heading reward is in $[-1, 0]$. Such normalisations make it easier to interpret the agent’s final performance and stabilise the training process. The third reward constituent penalises the collision risk by considering all other vessels via $r_{\text{coll},t} = \sum_{i=1}^{N_t} r_{\text{coll},i,t}$, where

the component for TS i is

$$r_{\text{coll},i,t} = \begin{cases} c_9 & \text{if } CR_{i,t} = 1, \\ -\sqrt{CR_{i,t}} & \text{otherwise,} \end{cases}$$

where $c_9 = -10$. Using the square root in the reward calculation deviates from prior linear suggestions, e.g. Chun et al. (2021). We found this adjustment useful because, since $CR_{i,t} \in [0, 1]$, it penalises the risk of a collision earlier and incentivises the agent to develop a more foresighted behaviour. Furthermore, we include a large negative penalty in the case of a collision.

The fourth component is responsible for COLREG compliance since it penalises the agent if it does not turn right in the head-on and starboard crossing situations for vessels for which the CPA has not been passed yet. We set $r_{\text{COLREG},t} = \sum_{i=1}^{N_t} r_{\text{COLREG},i,t}$, with the component for TS i being

$$r_{\text{COLREG},i,t} = \begin{cases} c_{10} & \text{if } \text{TCPA}_{i,t} \geq 0 \text{ and } \tilde{r}_t < 0 \text{ and } \sigma_{i,t} \in \{1, 2\}, \\ 0 & \text{otherwise,} \end{cases}$$

for the constant $c_{10} = -1$. We chose the yaw rate as a criterion instead of the rudder angle (as in Xu et al. (2020)) since the yaw rate is, by definition, the change in the heading and quantifies the actual turning of the ship’s nose. In ship dynamics, there can be a delay of several time steps in the translation from a sign change in the rudder angle to a sign change in the yaw rate, making the rudder angle less useful when it comes to judging whether a ship turns correctly.

The final reward quantity is an adaptive comfort reward that penalises steering if there is no or only a small risk of collision. Precisely, we have

$$r_{\text{comf},t} = \begin{cases} c_{11} & \text{if } a_t \neq 0 \text{ and } \forall i \in 1, \dots, N_t : CR_{i,t} \leq c_{12}, \\ 0 & \text{otherwise,} \end{cases} \quad (8)$$

where we set $c_{11} = -1$ and $c_{12} = 0.2$ in our simulation. We want to achieve a moderate and practically possible steering behaviour with the comfort reward, which avoids a non-human succession of very frequent course alterations. The total reward at a step t is constructed as follows:

$$r_t = r_{\text{dist},t}w_{\text{dist}} + r_{\text{head},t}w_{\text{head}} + r_{\text{coll},t}w_{\text{coll}} + r_{\text{COLREG},t}w_{\text{COLREG}} + r_{\text{comf},t}w_{\text{comf}},$$

for weights $w_{\text{dist}} = \frac{0.05}{6.15} \approx 0.0081$, $w_{\text{head}} = \frac{2.0}{6.15} \approx 0.3252$, $w_{\text{coll}} = \frac{1.8}{6.15} \approx 0.2927$, $w_{\text{COLREG}} = \frac{2.0}{6.15} \approx 0.3252$, and $w_{\text{comf}} = \frac{0.3}{6.15} \approx 0.0488$. The weights have been identified experimentally by running a grid search over different configurations.

5. Training

5.1. Environmental setup

We consider a simulation environment with $x_n, y_n \in [-7 \text{ NM}, 7 \text{ NM}]$. First, we uniformly sample an OS heading from $\{0, \frac{\pi}{2}, \pi, \frac{3}{2}\pi\}$. Then, the position of the OS in $\{n\}$ is set so that after 25 minutes in simulation time, it is at $o_n = (0, 0)$ if no steering takes place. The goal coordinate is initiated at the same distance but mirrored on o_n . Once the OS and goal are set, to improve generalisation, we randomly disturb the OS’s heading using a realisation of a uniform distribution $\mathcal{U}(-5^\circ, 5^\circ)$. Figure 7 shows the possible constellations of the OS and the goal.

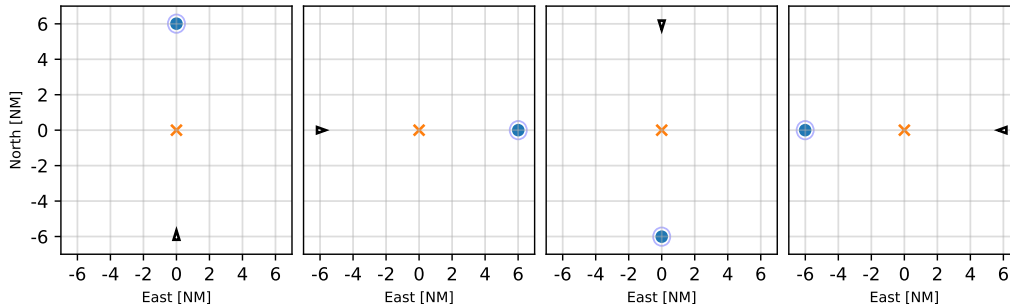


Figure 7: OS and goal spawning constellations. The black triangle is the OS, the orange cross is o_n , and the blue dot is the goal. The blue circle around the goal indicates the area (with radius $3L_{pp}$) that we consider as reaching the goal.

To generate the target vessels, we randomly sample a number of target ships from $\{0, 1, 2, 3\}$ with probabilities $\{0.1, 0.3, 0.3, 0.3\}$ to develop a robust and general final agent. Then, we run the following COLREG-based routine for initiating a vessel:

- First, we uniformly sample a COLREG situation $\sigma \in \{0, 1, 2, 3, 4\}$ and a corresponding heading intersection angle from the intervals in Table 1. If $\sigma = 0$, the null case, we randomly generate this angle from

$\mathcal{U}(-67.5^\circ, 67.5^\circ)$, which constructs a ship with a course similar to that of the OS. We found the inclusion of this case crucial since such cases do not otherwise appear when a COLREG-dependent spawning procedure is used.

- Second, we sample a propeller movement from $\mathcal{U}(0.9, 1.1) \cdot 1.8$ revolutions per second, guaranteeing the existence of slower and faster ships compared to the OS. Some prior researchers, e.g. Zhai et al. (2022), initiated all vessels at low or zero speed, which results in an acceleration phase with increased vessel manoeuvrability. We avoid this simplifying procedure by solving the system of equations (2) for the longitudinal speed u (fixing $v = r = 0$) and initialise the speed of the TS to the resulting value. The same procedure is used for the OS. Furthermore, when $\sigma = 4$ (overtaking), we multiply the derived speed of the TS by a realisation from $\mathcal{U}(0.3, 0.7)$, ensuring that the vessel is slow enough to be overtaken.
- Third, with the angle and velocity of the TS, we determine its position in $\{n\}$ by sampling a time t_0 from $\mathcal{U}(0.75, 1.0) \cdot 25$ minutes. The OS’s advancement in the goal direction during t_0 is computed by determining the relative velocity of the OS towards the goal and forecasting this velocity over t_0 . The procedure yields a point (x_{n,t_0}, y_{n,t_0}) . The TS is initiated after time t_0 at (x_{n,t_0}, y_{n,t_0}) , creating the need for the OS to steer and avoid a collision. This is contrary to prior work, e.g. that of Xu et al. (2022a), in which multiple target ships are randomly spawned in a simulation environment, resulting in the possibility of not creating a threat to the OS.

Figure 8 visualises exemplary scenarios in the case of one TS. An episode ends if the goal is reached or the number of episode steps is 1500. Crucially, we do not consider a collision an episode-ending event during training since we want to increase the number of highly negative reward transition tuples in the replay buffer. Recent research involving other traffic simulations (Wurman et al., 2022) shows that focusing on high-risk scenarios improves the robustness of the converged policy.

5.2. Algorithm configuration and results

We run the algorithm of subsection 4.2 for 10^7 steps. Table 2 shows the hyperparameters, while the source code is accessible at <https://github.com/>

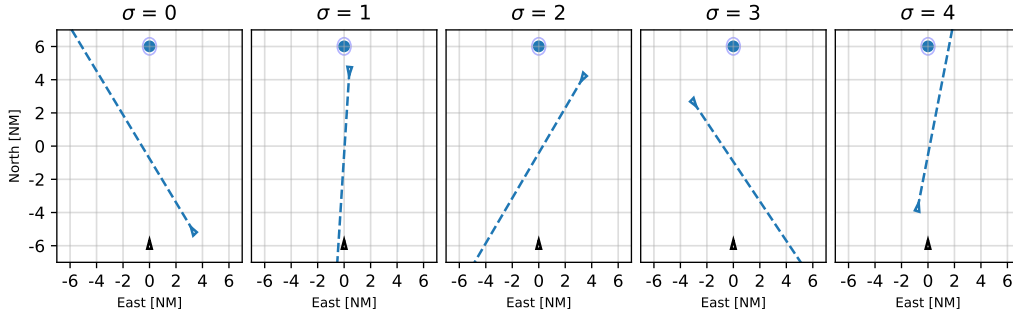


Figure 8: Sample of possible one-ship encounters during training.

MarWaltz/TUD_RL. During training, every 5,000 steps, we compute the sum of rewards, called the test return, of 10 evaluation episodes, average them, and exponentially smooth the results for clarity. Figure 9 displays the training performance, which shows a relatively stable improvement over the considered time steps.

Hyperparameter	Value
Batch size	32
Discount factor (γ)	0.999
Loss function	Mean squared error
Min. replay buffer size	1,000
Max. replay buffer size	10^5
Optimiser	Adam (Kingma and Ba, 2014)
Target network update frequency	1,000
Initial exploration rate ($\epsilon_{\text{initial}}$)	1.0
Final exploration rate (ϵ_{final})	0.1
Test exploration rate (ϵ_{test})	0.0
Exploration steps	10^6
Time steps	10^7
History length (h)	2

Table 2: List of hyperparameters. The ϵ value of the ϵ -greedy exploration scheme, which selects a random action with a probability ϵ and selects a greedy action otherwise, starts at 1.0 and linearly decays over 10^6 steps to a final value of 0.1.

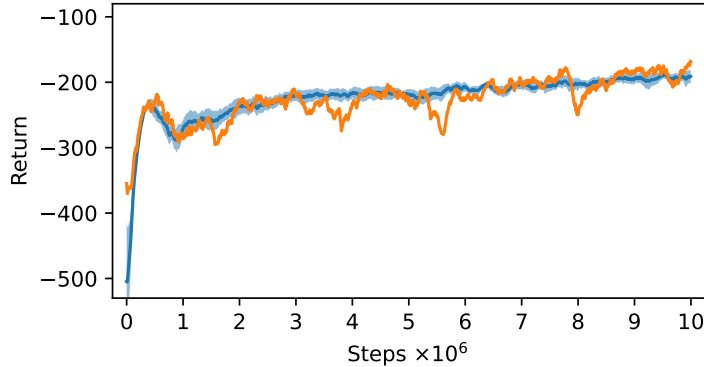


Figure 9: Test return over the training steps. The orange curve is the original run, which is used for validation. For comparison, we repeat the training and construct the blue curve, which represents a mean over 15 independent seeds. The shaded area around the blue curve depicts 95% point-wise confidence intervals and shows the algorithm’s stability.

6. Validation

6.1. Baselines

To assess the performance of our trained agent, we evaluate it in a range of scenarios involving single and multiple ships. To provide a benchmark for comparison, we choose two commonly used maritime path-planning techniques as baselines: the APF approach of Lyu and Yin (2019) and the VO method of Kuwata et al. (2014). These works were selected because they are the seminal maritime implementations of the APF and VO methods, which are among the most widely applied techniques in the field, as recently reported by Öztürk et al. (2022). Their corresponding hyperparameters are provided in Appendix B.

Our DRL approach combines local path planning and path following by controlling the rudder angle while considering the ship’s dynamics. On the other hand, the APF and VO methods only perform local path planning and directly adjust the heading of the OS. These latter methods require a separate low-level control module to execute the planned trajectory, which can impact their performance in practice. Despite these differences, we include plots of the trajectories generated by all three approaches in the following figures. This allows for a comprehensive comparison of their planning abilities in the context of our study.

6.2. Around the Clock

Regarding single-ship situations, we create the 24 Around the Clock problems. These situations correspond to 24 equally spaced TS headings in the interval $(0, 2\pi)$. Precisely, we have $\phi_{TS,j} = \frac{j}{25} \cdot 2\pi$ for $j = 1, \dots, 24$, where j is the case number. Similar to subsection 5.1, we initialise the OS and TS to be at $o_n = (0, 0)$ after 25 minutes and place the goal on the opposite side of the simulation area. The revolutions per second value is equal to 1.8 for all vessels. Figures 10 and 11 show the trajectories and the OS’s rudder angle, respectively, while the distances between the OS and the TS are depicted in Figure C.1 in Appendix C.

Upon analysing the trajectories generated by the DRL agent, we can observe that the agent successfully navigated to the goal while avoiding collisions with the linearly moving target ship. In all cases, the minimum encounter distance between the ships was greater than zero, demonstrating the effectiveness of the agent’s COLAV strategy. Notably, in cases 1–6, the agent opted to execute a turning manoeuvre in order to maintain a safe distance from the other vessel, showcasing its ability to proactively avoid potential collisions. In later scenarios, the agent selected right-steering manoeuvres that were compliant with COLREG regulations, such as in case 16, when it avoided a starboard-crosser. In the final case, the agent made the interesting decision to immediately turn to the starboard side to allow the target ship to pass and then resumed its course towards the goal when the target ship was safely out of range.

In all of the test scenarios, both the APF and VO approaches were able to successfully navigate without any collisions. However, the APF method exhibited some weaknesses in the first four cases; it suggested a path parallel to the target ship due to the superposition of attractive and repulsive forces. The VO approach performed better overall but still exhibited behaviour similar to that of the APF method in case 1, albeit to a lesser degree. One of the primary drawbacks of the VO method is the potential for bow-crossing with a target ship, which is seen in cases 3 and 6 and is generally considered to be unsafe in practice. In contrast, the DRL agent was able to avoid this behaviour entirely through the use of turning manoeuvres.

In addition, the steering behaviour of the DRL agent is generally moderate, although there are some instances – such as cases 7 and 8 – in which the agent selects a sequence of alternating large positive and negative rudder angles. However, since each trajectory corresponds to over an hour of real time, these manoeuvres are still within the range of realistic behaviour. Notably, in

case 24, the agent was able to maintain a steady course towards the goal for nearly half an hour without making any steering adjustments, demonstrating its ability to navigate successfully in the absence of any critical target ships.

6.3. Imazu problems

The second set of validation scenarios contains the Imazu problems (Imazu, 1987; Sawada et al., 2021; Zhai et al., 2022), a collection of single- and multi-ship encounters. The initial constellations of the target ships are detailed in Table D.1 of Appendix D, while Figures 12, 13, and 14 show the trajectories, the distances between the OS and the target ships, and the rudder angles of the agent, respectively. Similar to the Around the Clock scenarios, the DRL agent smoothly reaches the desired goal area while successfully avoiding collisions with target ships for all problems. Moreover, the COLREG compliance of the ship is shown since the agent avoids head-on target ships and starboard-crossers by steering to the right; see, e.g. cases 1, 2, 19, and 22. Moreover, following rule 8 of the COLREGs, the agent takes *substantial* COLAV actions in these cases, which result in a sufficient perception of the agent’s steering behaviour when there are other ships in a situation at sea. Additionally, we do not observe any undesired bow-crossing of the target ships, indicating the benefit of incorporating the factor f_{DCPA} in (6).

An interesting characteristic of the DRL agent’s steering behaviour is the frequent use of turning manoeuvres. In the five cases 4, 10, 11, 13, and 16, the OS performs a starboard turn, which occurs at different times throughout the respective episode depending on the distance to the relevant TS. Such an advanced turning manoeuvre was also observed by Sawada et al. (2021), whose agent performed a starboard turn only in case 4 of the same problem set. The authors attributed the ability to perform such a turning manoeuvre to the specification of a continuous action space in the RL algorithm. However, due to our spatial-temporal recurrent neural architecture, we realise an efficient information-processing procedure that still allows such a manoeuvre with our simple, discrete action space.

When comparing the three implemented methods, it is evident that the APF approach is the least effective at handling the encountered scenarios. As in the single-ship validations, the APF method often becomes trapped in a parallel situation next to a target ship, resulting in suboptimal paths and potentially unsafe situations. Additionally, the APF method struggles with symmetrical situations and can even lead to collisions in scenarios such as

cases 19 and 21, where two closely positioned target ships are present from the start. On the other hand, the VO method performs much better and generally finds a short and collision-free path. However, as seen in cases 4, 6, and 13, it can still result in unsafe bow-crossing behaviour, which could pose a problem in real-life scenarios.

Interestingly, the rudder movement plot (Figure 14) indicates that the DRL agent exhibits a low frequency of steering actions, with long phases with no steering at all, as seen in cases 11 and 18. Despite this, the agent still successfully navigated the complex scenarios presented in the validation, highlighting the effectiveness of the developed policy in handling real-world situations. Overall, the results demonstrate that our DRL approach offers advantages in terms of robustness and safety, and has the potential to be a valuable tool for practical path planning and COLAV applications in maritime environments.

6.4. *Star problems*

The training and validation scenarios presented so far have assumed a deterministic linear motion for the target ships, which is unrealistic in practice but common in the literature (Guo et al., 2020; Fan et al., 2022; Xu et al., 2022a). To ensure that our final DRL policy can handle non-linear target ship movements, we tested it on two challenging multi-ship encounter scenarios known as Star problems (Zhao and Roh, 2019). The scenarios consist of four and eight ships, respectively, and the initial headings are spaced over $[0, 2\pi)$. Each ship is set to reach the origin $(0, 0)$ after 25 minutes if no steering takes place. Figure 15 shows the resulting trajectories, where each ship’s goal is to reach the opposite ship’s spawning area while following the same policy validated in previous subsections.

Remarkably, the DRL policy successfully navigates through both scenarios, steering each ship to the right and then to the left to avoid collisions and reach the goal. In the eight-ship scenario, the COLAV actions are more intense, and the ships follow a more conservative, nearly circular path, reflecting the riskiness of a situation with so many vessels. These tasks are particularly challenging since the agent has never encountered more than three target ships in training nor was it ever exposed to non-linear moving ships. The policy’s ability to handle such complex requirements demonstrates the neural architecture’s flexibility and suitability for real-world maritime traffic applications.

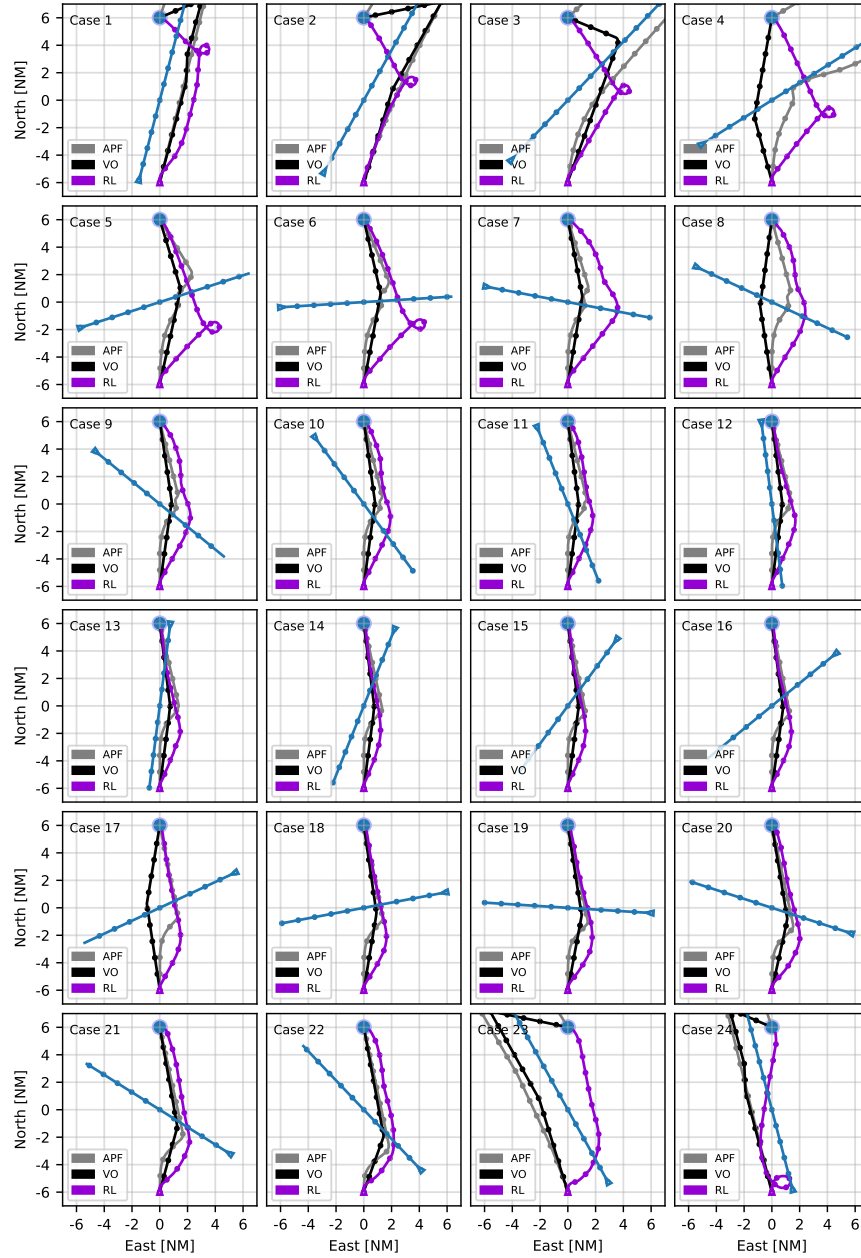


Figure 10: Around the Clock trajectories. The target ship trajectories are blue. Two consecutive dots on a trajectory correspond to a 5-minute time interval.

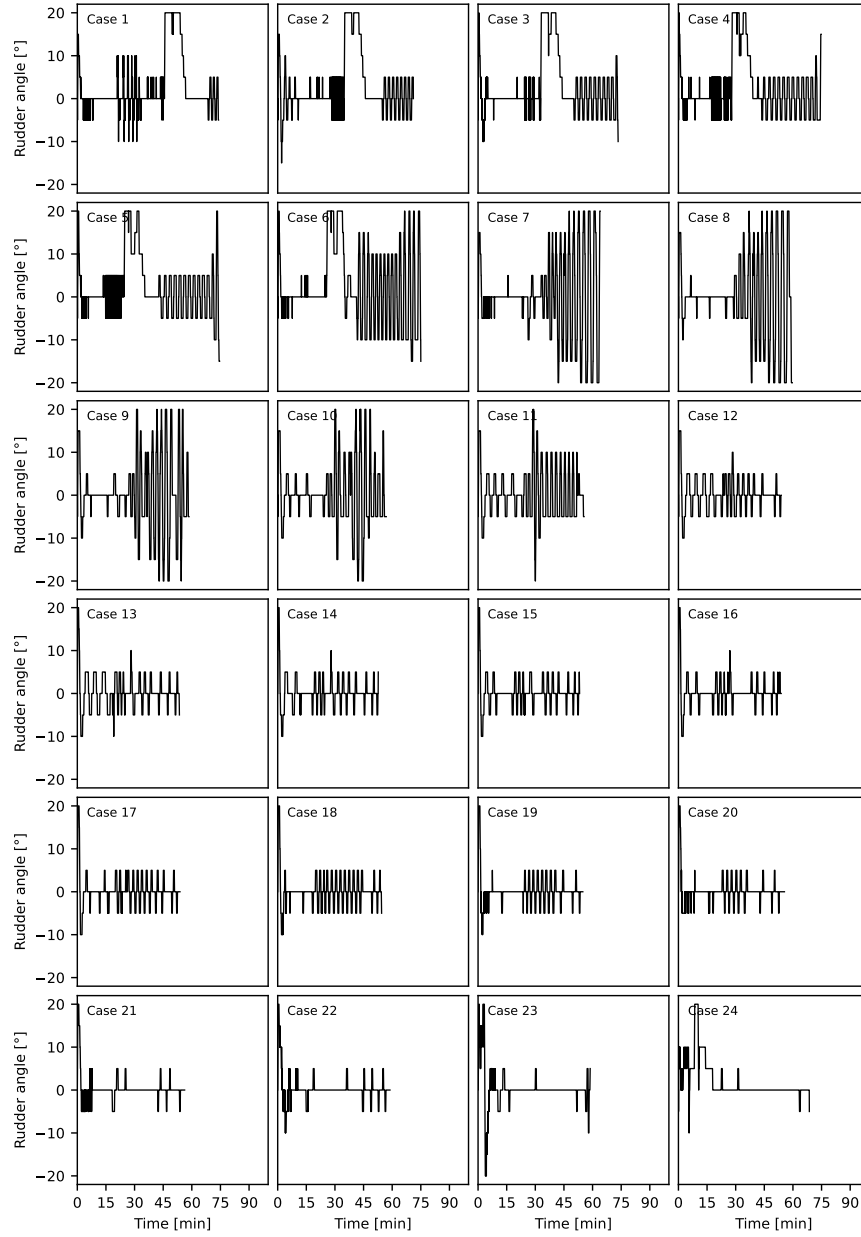


Figure 11: Rudder angles of the DRL agent during the Around the Clock scenarios.

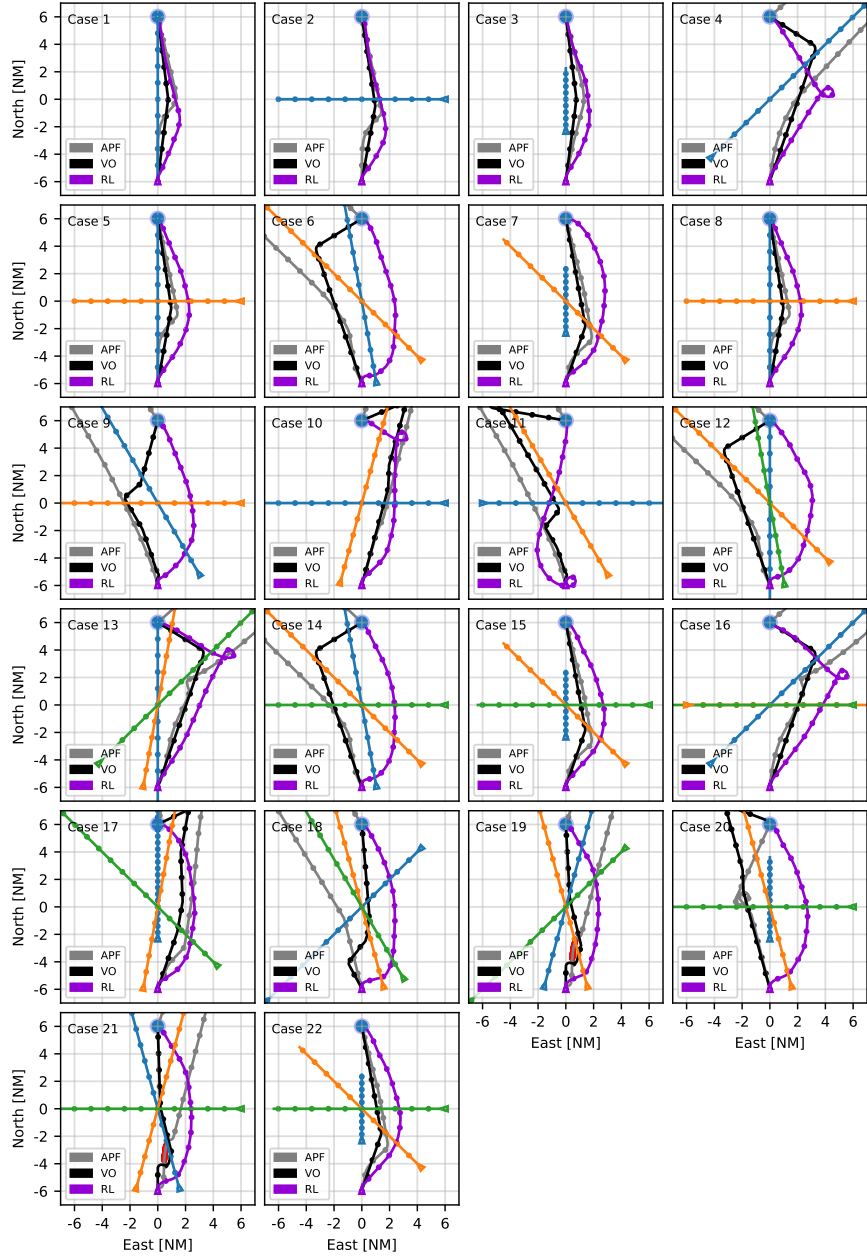


Figure 12: Trajectories for the Imazu problems. The blue, orange, and green trajectories represent target ships, while a red area indicates a collision. Two consecutive dots on a trajectory correspond to a 5-minute time interval.

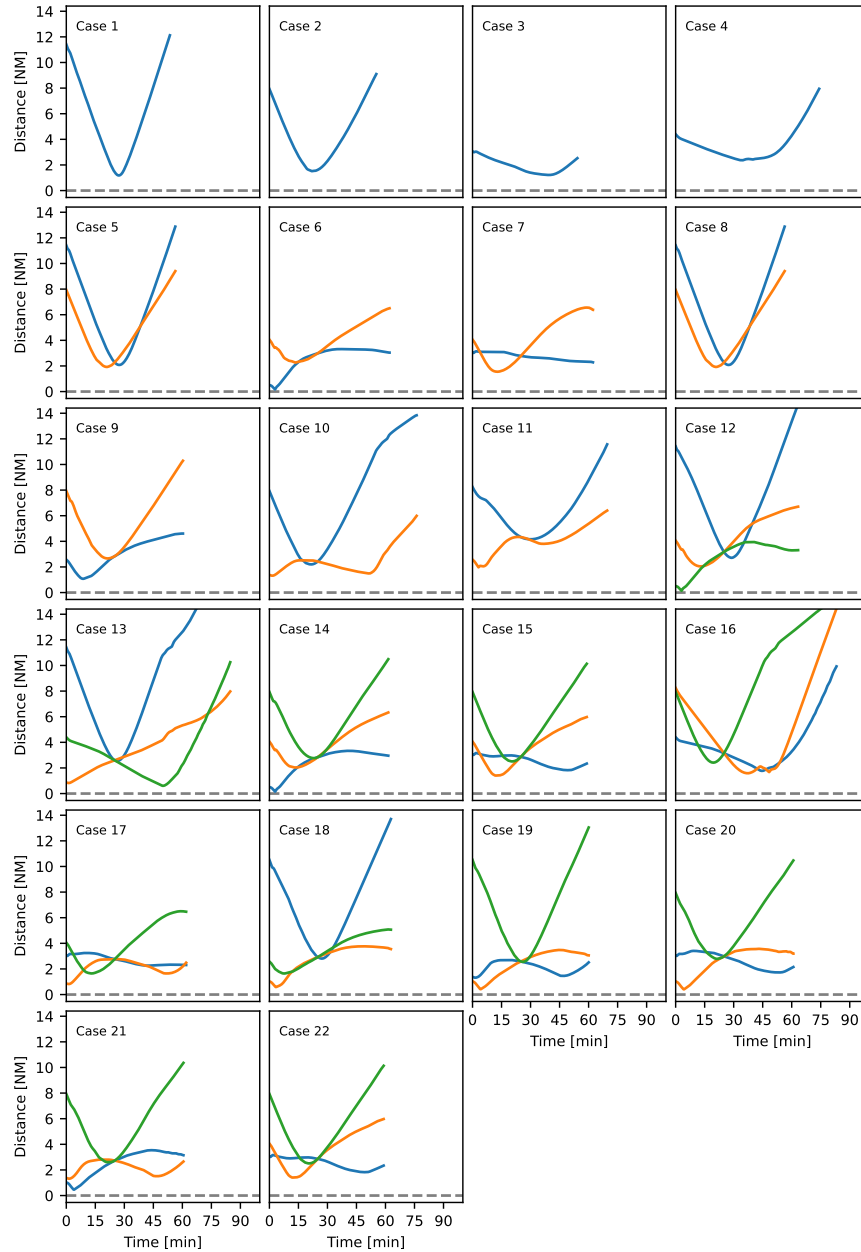


Figure 13: Distances of the DRL agent to the target ships for the Imazu problems. A distance of zero is not a physical collision; it indicates that the target ship is exactly at the border of the agent's ship domain.

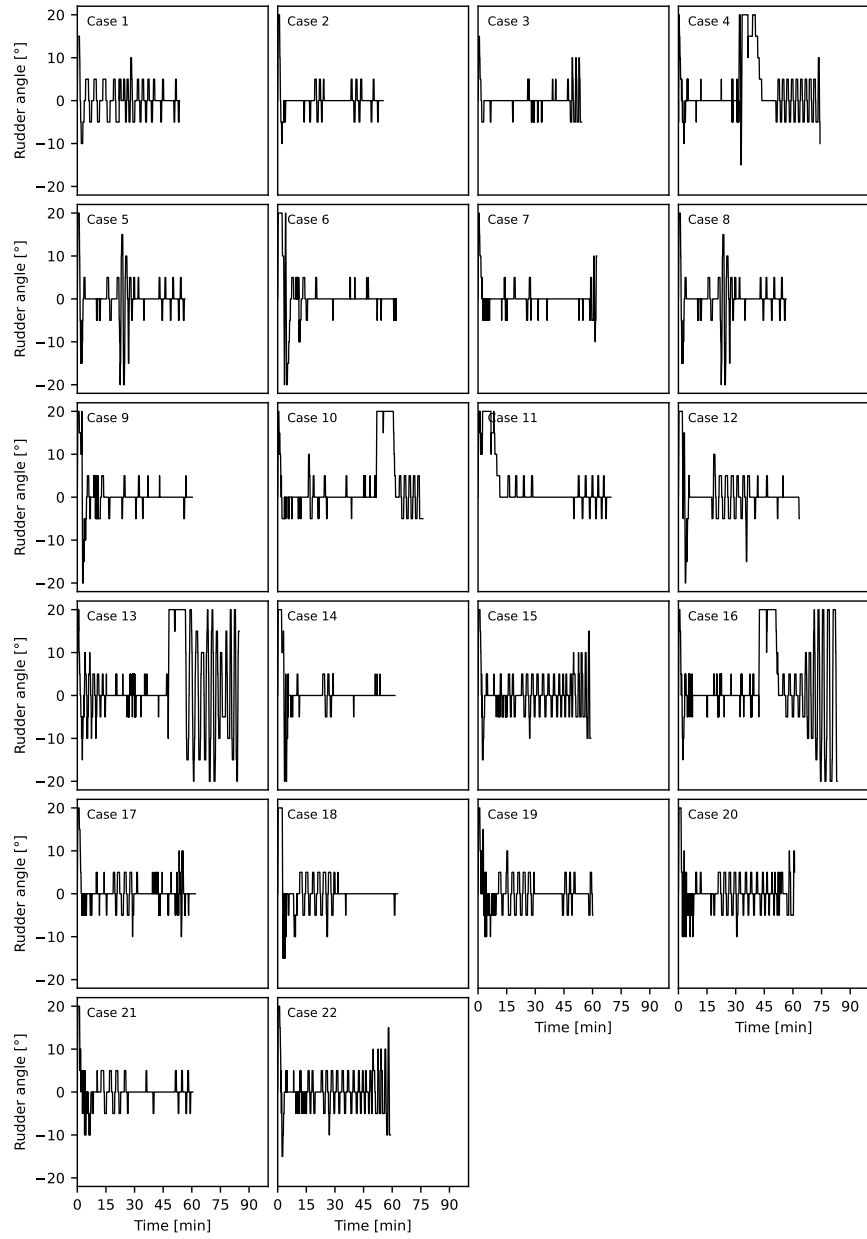


Figure 14: Steering behaviour of the DRL agent for the Imazu problems.

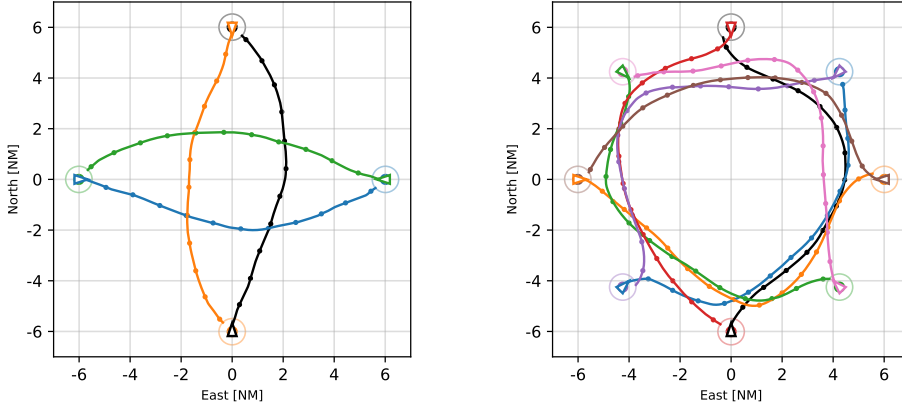


Figure 15: Validation on the Star problems. Each ship represents a DRL agent and follows the same policy. The objective is to reach the opposite side of the grid.

7. Conclusion

Artificial intelligence has the potential to enhance safety, reduce accidents, and save energy resources in critical domains by either assisting or performing human actions. One such domain is maritime traffic, where technological advancements in ASV design coupled with regulatory adjustments could revolutionise how we perceive sea traffic. This study presents an ASV agent using deep Q-networks with a spatial-temporal recurrent neural network architecture to create a robust policy. The approach is validated on realistic multi-ship encounters, and it generates practically viable steering decisions aided by a newly proposed collision risk metric. In summary, our method has several advantages, including the ability to handle an arbitrary number of target ships, robustness to partial observability, state-of-the-art collision risk assessment, compliance with maritime traffic rules, and computational efficiency, making it feasible for practical deployment.

Despite the success of our agent, there are limitations that we aim to address in future research. First, we assume that environmental disturbances such as wind, waves, and currents are not present. Incorporating these forces into our simulation is essential to ensure that our agent can perform adequately in real-world scenarios. Second, our agent relies on AIS data to obtain information about surrounding ships, and it is unaware of environmental characteristics such as the water depth, static obstacles, and non-AIS-equipped traffic participants. A future fully autonomous ASV should

process additional sensor information and nautical maps to incorporate this information. Finally, all our work was performed in simulations, and we plan to conduct real-world experiments with miniature vessels to validate our architecture in the field.

Acknowledgments

The authors express their sincere gratitude to the anonymous reviewers for their valuable feedback, which significantly enhanced the quality of this manuscript. Additionally, the authors extend their thanks to Fabian Hart, Niklas Paulig, and Martin Treiber for their insightful comments and discussions. The authors also acknowledge the Center for Information Services and High Performance Computing at TU Dresden for providing the resources for high-throughput calculations, which greatly supported this research. This research did not receive any specific grant from funding agencies in the public, commercial, or not-for-profit sectors.

References

- Abdelaal, M., Fränzle, M., & Hahn, A. (2018). Nonlinear model predictive control for trajectory tracking and collision avoidance of underactuated vessels with disturbances. *Ocean Engineering*, 160:168–180.
- Akdağ, M., Solnør, P., & Johansen, T. A. (2022). Collaborative collision avoidance for maritime autonomous surface ships: A review. *Ocean Engineering*, 250:110920.
- Almalioglu, Y., Turan, M., Trigoni, N., & Markham, A. (2022). Deep learning-based robust positioning for all-weather autonomous driving. *Nature Machine Intelligence*, 4(9):749–760.
- Autoship (2023). Autonomous shipping initiative for European waters. <https://www.autoship-project.eu/>. Accessed April 3, 2023.
- Bellemare, M. G., Candido, S., Castro, P. S., Gong, J., Machado, M. C., Moitra, S., Ponda, S. S., & Wang, Z. (2020). Autonomous navigation of stratospheric balloons using reinforcement learning. *Nature*, 588(7836):77–82.

- Benjamin, M. R. (2017). Autonomous COLREGS modes and velocity functions. Technical report, Massachusetts Institute of Technology, Cambridge.
- Bertsekas, D. (2019). *Reinforcement learning and optimal control*. Athena Scientific.
- Breivik, M. et al. (2017). MPC-based mid-level collision avoidance for ASVs using nonlinear programming. In *2017 IEEE Conference on Control Technology and Applications*, pages 766–772. IEEE.
- Cheng, Y. & Zhang, W. (2018). Concise deep reinforcement learning obstacle avoidance for underactuated unmanned marine vessels. *Neurocomputing*, 272:63–73.
- Chiang, H.-T. L. & Tapia, L. (2018). COLREG-RRT: An RRT-based COLREGS-compliant motion planner for surface vehicle navigation. *IEEE Robotics and Automation Letters*, 3(3):2024–2031.
- Chun, D.-H., Roh, M.-I., Lee, H.-W., Ha, J., & Yu, D. (2021). Deep reinforcement learning-based collision avoidance for an autonomous ship. *Ocean Engineering*, 234:109216.
- D’Eramo, C., Cini, A., Nuara, A., Pirotta, M., Alippi, C., Peters, J., & Restelli, M. (2021). Gaussian approximation for bias reduction in Q-learning. *The Journal of Machine Learning Research*, 22(1):12690–12740.
- Du, Z., Negenborn, R. R., & Reppa, V. (2022). COLREGS-compliant collision avoidance for physically coupled multi-vessel systems with distributed MPC. *Ocean Engineering*, 260:111917.
- Enevoldsen, T. T., Reinartz, C., & Galeazzi, R. (2021). COLREGs-informed RRT* for collision avoidance of marine crafts. In *International Conference on Robotics and Automation*, pages 8083–8089. IEEE.
- Eriksen, B.-O. H., Bitar, G., Breivik, M., & Lekkas, A. M. (2020). Hybrid collision avoidance for ASVs compliant with COLREGs rules 8 and 13–17. *Frontiers in Robotics and AI*, 7:11.
- European Maritime Safety Agency (2021). Annual overview of marine casualties and incidents. <https://www.emsa.europa.eu/newsroom/latest-news/download/6955/4266/23.html>. Accessed September 26, 2022.

- Everett, M., Chen, Y. F., & How, J. P. (2018). Motion planning among dynamic, decision-making agents with deep reinforcement learning. In *International Conference on Intelligent Robots and Systems*, pages 3052–3059. IEEE.
- Everett, M., Chen, Y. F., & How, J. P. (2021). Collision avoidance in pedestrian-rich environments with deep reinforcement learning. *IEEE Access*, 9:10357–10377.
- Fan, Y., Sun, Z., & Wang, G. (2022). A novel reinforcement learning collision avoidance algorithm for USVs based on maneuvering characteristics and COLREGs. *Sensors*, 22(6):2099.
- Fiorini, P. & Shiller, Z. (1998). Motion planning in dynamic environments using velocity obstacles. *The International Journal of Robotics Research*, 17(7):760–772.
- Fossen, T. I. (2021). *Handbook of marine craft hydrodynamics and motion control (2nd ed.)*. John Wiley & Sons.
- Fujimoto, S., Hoof, H., & Meger, D. (2018). Addressing function approximation error in actor-critic methods. In *International Conference on Machine Learning*, pages 1587–1596. PMLR.
- Gao, Z., Cecati, C., & Ding, S. X. (2015). A survey of fault diagnosis and fault-tolerant techniques—Part I: Fault diagnosis with model-based and signal-based approaches. *IEEE Transactions on Industrial Electronics*, 62(6):3757–3767.
- Garcia, C. E., Prett, D. M., & Morari, M. (1989). Model predictive control: Theory and practice—A survey. *Automatica*, 25(3):335–348.
- Ge, S. S. & Cui, Y. J. (2000). New potential functions for mobile robot path planning. *IEEE Transactions on Robotics and Automation*, 16(5):615–620.
- Goodwin, E. M. (1975). A statistical study of ship domains. *The Journal of Navigation*, 28(3):328–344.
- Guo, S., Zhang, X., Zheng, Y., & Du, Y. (2020). An autonomous path planning model for unmanned ships based on deep reinforcement learning. *Sensors*, 20(2):426.

- Ha, J., Roh, M.-I., & Lee, H.-W. (2021). Quantitative calculation method of the collision risk for collision avoidance in ship navigation using the CPA and ship domain. *Journal of Computational Design and Engineering*, 8(3):894–909.
- Hagen, I. B., Kufoalor, D. K. M., Brekke, E. F., & Johansen, T. A. (2018). MPC-based collision avoidance strategy for existing marine vessel guidance systems. In *International Conference on Robotics and Automation*, pages 7618–7623. IEEE.
- Hart, F., Okhrin, O., & Treiber, M. (2022). Vessel-following model for inland waterways based on deep reinforcement learning. *arXiv preprint. arXiv:2207.03257*.
- Heess, N., Hunt, J. J., Lillicrap, T. P., & Silver, D. (2015). Memory-based control with recurrent neural networks. *arXiv preprint. arXiv:1512.04455*.
- Heiberg, A., Larsen, T. N., Meyer, E., Rasheed, A., San, O., & Varagnolo, D. (2022). Risk-based implementation of COLREGs for autonomous surface vehicles using deep reinforcement learning. *Neural Networks*, 152:17–33.
- Hessel, M., Modayil, J., Van Hasselt, H., Schaul, T., Ostrovski, G., Dabney, W., Horgan, D., Piot, B., Azar, M., & Silver, D. (2018). Rainbow: Combining improvements in deep reinforcement learning. In *AAAI Conference on Artificial Intelligence*, volume 32.
- Hochreiter, S. & Schmidhuber, J. (1997). Long short-term memory. *Neural Computation*, 9(8):1735–1780.
- Holland, J. H. (1992). *Adaptation in natural and artificial systems: An introductory analysis with applications to biology, control, and artificial intelligence*. MIT Press.
- Huang, Y., Chen, L., Chen, P., Negenborn, R. R., & Van Gelder, P. (2020). Ship collision avoidance methods: State-of-the-art. *Safety Science*, 121:451–473.
- Huang, Y., Chen, L., & Van Gelder, P. (2019). Generalized velocity obstacle algorithm for preventing ship collisions at sea. *Ocean Engineering*, 173:142–156.

- Huang, Y., Van Gelder, P., & Wen, Y. (2018). Velocity obstacle algorithms for collision prevention at sea. *Ocean Engineering*, 151:308–321.
- Imazu, H. (1987). *Research on collision avoidance manoeuvre*. PhD thesis, The University of Tokyo.
- International Maritime Organization (1972). *COLREG: Convention on the International Regulations for Preventing Collisions at Sea*.
- Johansen, T. A., Perez, T., & Cristofaro, A. (2016). Ship collision avoidance and COLREGS compliance using simulation-based control behavior selection with predictive hazard assessment. *IEEE Transactions on Intelligent Transportation Systems*, 17(12):3407–3422.
- Ju, H., Juan, R., Gomez, R., Nakamura, K., & Li, G. (2022). Transferring policy of deep reinforcement learning from simulation to reality for robotics. *Nature Machine Intelligence*, pages 1–11.
- Kaelbling, L. P., Littman, M. L., & Cassandra, A. R. (1998). Planning and acting in partially observable stochastic domains. *Artificial Intelligence*, 101(1-2):99–134.
- Kang, Y.-T., Chen, W.-J., Zhu, D.-Q., & Wang, J.-H. (2021). Collision avoidance path planning in multi-ship encounter situations. *Journal of Marine Science and Technology*, 26(4):1026–1037.
- Karaman, S. & Frazzoli, E. (2011). Sampling-based algorithms for optimal motion planning. *The International Journal of Robotics Research*, 30(7):846–894.
- Khatib, O. (1985). Real-time obstacle avoidance for manipulators and mobile robots. In *International Conference on Robotics and Automation*, volume 2, pages 500–505.
- Kim, H., Kim, S.-H., Jeon, M., Kim, J., Song, S., & Paik, K.-J. (2017). A study on path optimization method of an unmanned surface vehicle under environmental loads using genetic algorithm. *Ocean Engineering*, 142:616–624.
- Kingma, D. P. & Ba, J. (2014). Adam: A method for stochastic optimization. *arXiv preprint. arXiv:1412.6980*.

- Kongsberg (2023). Autonomous ship project, key facts about Yara Birkeland. <https://www.kongsberg.com/no/maritime/support/themes/autonomous-ship-project-key-facts-about-yara-birkeland/>. Accessed April 3, 2023.
- Kuffner, J. J. & LaValle, S. M. (2000). RRT-connect: An efficient approach to single-query path planning. In *International Conference on Robotics and Automation*, volume 2, pages 995–1001. IEEE.
- Kuwata, Y., Wolf, M. T., Zarzhitsky, D., & Huntsberger, T. L. (2014). Safe maritime autonomous navigation with COLREGS, using velocity obstacles. *IEEE Journal of Oceanic Engineering*, 39(1):110–119.
- LaValle, S. M. & Kuffner Jr, J. J. (2001). Randomized kinodynamic planning. *The International Journal of Robotics Research*, 20(5):378–400.
- Lazarowska, A. (2015). Ship’s trajectory planning for collision avoidance at sea based on ant colony optimisation. *The Journal of Navigation*, 68(2):291–307.
- LeCun, Y., Bengio, Y., & Hinton, G. (2015). Deep learning. *Nature*, 521(7553):436–444.
- Lenart, A. S. (1983). Collision threat parameters for a new radar display and plot technique. *The Journal of Navigation*, 36(3):404–410.
- Li, L., Wu, D., Huang, Y., & Yuan, Z.-M. (2021). A path planning strategy unified with a COLREGS collision avoidance function based on deep reinforcement learning and artificial potential field. *Applied Ocean Research*, 113:102759.
- Lillicrap, T. P., Hunt, J. J., Pritzel, A., Heess, N., Erez, T., Tassa, Y., Silver, D., & Wierstra, D. (2015). Continuous control with deep reinforcement learning. *arXiv preprint. arXiv:1509.02971*.
- Lin, B. & Huang, C.-H. (2006). Comparison between ARPA radar and AIS characteristics for vessel traffic services. *Journal of Marine Science and Technology*, 14(3):7.

- Liu, W., Qiu, K., Yang, X., Wang, R., Xiang, Z., Wang, Y., & Xu, W. (2023). COLREGS-based collision avoidance algorithm for unmanned surface vehicles using modified artificial potential fields. *Physical Communication*, 57:101980.
- Liu, Y., Bu, R., & Gao, X. (2018). Ship trajectory tracking control system design based on sliding mode control algorithm. *Polish Maritime Research*, 25(3):26–34.
- Liu, Y. & Bucknall, R. (2015). Path planning algorithm for unmanned surface vehicle formations in a practical maritime environment. *Ocean Engineering*, 97:126–144.
- Liu, Z., Zhang, Y., Yu, X., & Yuan, C. (2016). Unmanned surface vehicles: An overview of developments and challenges. *Annual Reviews in Control*, 41:71–93.
- Lyu, H. & Yin, Y. (2018). Fast path planning for autonomous ships in restricted waters. *Applied Sciences*, 8(12):2592.
- Lyu, H. & Yin, Y. (2019). COLREGS-constrained real-time path planning for autonomous ships using modified artificial potential fields. *The Journal of Navigation*, 72(3):588–608.
- Matsuo, Y., LeCun, Y., Sahani, M., Precup, D., Silver, D., Sugiyama, M., Uchibe, E., & Morimoto, J. (2022). Deep learning, reinforcement learning, and world models. *Neural Networks*, 152:267–275.
- Meng, L., Gorbet, R., & Kulić, D. (2021). Memory-based deep reinforcement learning for POMDPs. In *International Conference on Intelligent Robots and Systems*, pages 5619–5626. IEEE.
- Meyer, E., Robinson, H., Rasheed, A., & San, O. (2020). Taming an autonomous surface vehicle for path following and collision avoidance using deep reinforcement learning. *IEEE Access*, 8:41466–41481.
- Miyoshi, T., Fujimoto, S., Rooks, M., Konishi, T., & Suzuki, R. (2022). Rules required for operating maritime autonomous surface ships from the viewpoint of seafarers. *The Journal of Navigation*, 75(2):384–399.

- Mnih, V., Kavukcuoglu, K., Silver, D., Rusu, A. A., Veness, J., Bellemare, M. G., Graves, A., Riedmiller, M., Fidjeland, A. K., Ostrovski, G., et al. (2015). Human-level control through deep reinforcement learning. *Nature*, 518(7540):529–533.
- Mou, J. M., Van Der Tak, C., & Ligteringen, H. (2010). Study on collision avoidance in busy waterways by using AIS data. *Ocean Engineering*, 37(5-6):483–490.
- Nelson, D. R., Barber, D. B., McLain, T. W., & Beard, R. W. (2007). Vector field path following for miniature air vehicles. *IEEE Transactions on Robotics*, 23(3):519–529.
- Ning, J., Chen, H., Li, T., Li, W., & Li, C. (2020). COLREGs-compliant unmanned surface vehicles collision avoidance based on multi-objective genetic algorithm. *IEEE Access*, 8:190367–190377.
- Öztürk, Ü., Akdağ, M., & Ayabakan, T. (2022). A review of path planning algorithms in maritime autonomous surface ships: Navigation safety perspective. *Ocean Engineering*, 251:111010.
- Öztürk, Ü. & Cicek, K. (2019). Individual collision risk assessment in ship navigation: A systematic literature review. *Ocean Engineering*, 180:130–143.
- Paszke, A., Gross, S., Massa, F., Lerer, A., Bradbury, J., Chanan, G., Killeen, T., Lin, Z., Gimelshein, N., Antiga, L., Desmaison, A., Köpf, A., Yang, E., DeVito, Z., Raison, M., Tejani, A., Chilamkurthy, S., Steiner, B., Fang, L., Bai, J., & Chintala, S. (2019). PyTorch: An imperative style, high-performance deep learning library. *Advances in Neural Information Processing Systems*, 32:8026–8037.
- Paulig, N. & Okhrin, O. (2023). Robust path following on rivers using bootstrapped reinforcement learning. *arXiv preprint. arXiv:2303.15178*.
- Puterman, M. L. (1994). *Markov decision processes: Discrete stochastic dynamic programming*. John Wiley & Sons.
- Ribeiro, M., Ellerbroek, J., & Hoekstra, J. (2021). Velocity obstacle based conflict avoidance in urban environment with variable speed limit. *Aerospace*, 8(4):93.

- Rolls-Royce (2015). Advanced autonomous waterborne applications initiative. <https://www.rolls-royce.com/media/press-releases/2015/pr-02-07-15-rolls-royce-to-lead-autonomous-ship-research-project.aspx>. Accessed April 3, 2023.
- Sandeepkumar, R., Rajendran, S., Mohan, R., & Pascoal, A. (2022). A unified ship manoeuvring model with a nonlinear model predictive controller for path following in regular waves. *Ocean Engineering*, 243:110165.
- Sawada, R., Sato, K., & Majima, T. (2021). Automatic ship collision avoidance using deep reinforcement learning with LSTM in continuous action spaces. *Journal of Marine Science and Technology*, 26(2):509–524.
- Schaul, T., Quan, J., Antonoglou, I., & Silver, D. (2015). Prioritized experience replay. *arXiv preprint. arXiv:1511.05952*.
- Schulman, J., Wolski, F., Dhariwal, P., Radford, A., & Klimov, O. (2017). Proximal policy optimization algorithms. *arXiv preprint. arXiv:1707.06347*.
- Serigstad, E., Eriksen, B.-O. H., & Breivik, M. (2018). Hybrid collision avoidance for autonomous surface vehicles. *IFAC-PapersOnLine*, 51(29):1–7.
- Shen, H., Hashimoto, H., Matsuda, A., Taniguchi, Y., Terada, D., & Guo, C. (2019). Automatic collision avoidance of multiple ships based on deep Q-learning. *Applied Ocean Research*, 86:268–288.
- Siciliano, B., Khatib, O., & Kröger, T. (2008). *Springer handbook of robotics*, volume 200. Springer.
- Silver, D., Singh, S., Precup, D., & Sutton, R. S. (2021). Reward is enough. *Artificial Intelligence*, 299:103535.
- Skjetne, R., Smogeli, Ø. N., & Fossen, T. I. (2004). A nonlinear ship manoeuvring model: Identification and adaptive control with experiments for a model ship. *Modeling, Identification and Control*, 25(1):3.
- Śmierczalski, R. (2005). Ships’ domains as collision risk at sea in the evolutionary method of trajectory planning. In *Information Processing and Security Systems*, pages 411–422. Springer.

- Stern, F., Agdraup, K., Kim, S., Hochbaum, A., Rhee, K., Quadvlieg, F., Perdon, P., Hino, T., Broglia, R., & Gorski, J. (2011). Experience from SIMMAN 2008—The first workshop on verification and validation of ship maneuvering simulation methods. *Journal of Ship Research*, 55(02):135–147.
- Sutton, R. S. & Barto, A. G. (2018). *Reinforcement learning: An introduction*. MIT Press.
- Szlapczynski, R. & Szlapczynska, J. (2017). Review of ship safety domains: Models and applications. *Ocean Engineering*, 145:277–289.
- Tam, C. & Bucknall, R. (2010). Path-planning algorithm for ships in close-range encounters. *Journal of Marine Science and Technology*, 15:395–407.
- Tang, W., Zhou, Y., Zhang, T., Liu, Y., Liu, J., & Ding, Z. (2023). Co-operative collision avoidance in multirobot systems using fuzzy rules and velocity obstacles. *Robotica*, 41(2):668–689.
- Tao, H., Qiu, J., Chen, Y., Stojanovic, V., & Cheng, L. (2023). Unsupervised cross-domain rolling bearing fault diagnosis based on time-frequency information fusion. *Journal of the Franklin Institute*, 360(2):1454–1477.
- Treiber, M. & Kanagaraj, V. (2015). Comparing numerical integration schemes for time-continuous car-following models. *Physica A: Statistical Mechanics and its Applications*, 419:183–195.
- Tsitsiklis, J. N. (1994). Asynchronous stochastic approximation and Q-learning. *Machine Learning*, 16(3):185–202.
- Vagale, A., Bye, R. T., Oucheikh, R., Osen, O. L., & Fossen, T. I. (2021a). Path planning and collision avoidance for autonomous surface vehicles II: A comparative study of algorithms. *Journal of Marine Science and Technology*, 26(4):1307–1323.
- Vagale, A., Oucheikh, R., Bye, R. T., Osen, O. L., & Fossen, T. I. (2021b). Path planning and collision avoidance for autonomous surface vehicles I: A review. *Journal of Marine Science and Technology*, 26:1292–1306.
- Van Hasselt, H., Guez, A., & Silver, D. (2016). Deep reinforcement learning with double Q-learning. In *AAAI Conference on Artificial Intelligence*, volume 30.

- Vinyals, O., Babuschkin, I., Czarnecki, W. M., Mathieu, M., Dudzik, A., Chung, J., Choi, D. H., Powell, R., Ewalds, T., Georgiev, P., et al. (2019). Grandmaster level in StarCraft II using multi-agent reinforcement learning. *Nature*, 575(7782):350–354.
- Vrabie, D., Pastravanu, O., Abu-Khalaf, M., & Lewis, F. L. (2009). Adaptive optimal control for continuous-time linear systems based on policy iteration. *Automatica*, 45(2):477–484.
- Waltz, M. & Okhrin, O. (2022). Two-sample testing in reinforcement learning. *arXiv preprint. arXiv:2201.08078*.
- Wang, C., Wang, J., Shen, Y., & Zhang, X. (2019). Autonomous navigation of UAVs in large-scale complex environments: A deep reinforcement learning approach. *IEEE Transactions on Vehicular Technology*, 68(3):2124–2136.
- Wang, H., Fu, Z., Zhou, J., Fu, M., & Ruan, L. (2021). Cooperative collision avoidance for unmanned surface vehicles based on improved genetic algorithm. *Ocean Engineering*, 222:108612.
- Wang, W., Shan, T., Leoni, P., Fernández-Gutiérrez, D., Meyers, D., Ratti, C., & Rus, D. (2020). Roboat II: A novel autonomous surface vessel for urban environments. In *International Conference on Intelligent Robots and Systems*, pages 1740–1747. IEEE.
- Wang, Z., Schaul, T., Hessel, M., Hasselt, H., Lanctot, M., & Freitas, N. (2016). Dueling network architectures for deep reinforcement learning. In *International Conference on Machine Learning*, pages 1995–2003. PMLR.
- Watkins, C. J. & Dayan, P. (1992). Q-learning. *Machine Learning*, 8(3):279–292.
- Woo, J. & Kim, N. (2020). Collision avoidance for an unmanned surface vehicle using deep reinforcement learning. *Ocean Engineering*, 199:107001.
- Woo, J., Yu, C., & Kim, N. (2019). Deep reinforcement learning-based controller for path following of an unmanned surface vehicle. *Ocean Engineering*, 183:155–166.

- Wurman, P. R., Barrett, S., Kawamoto, K., MacGlashan, J., Subramanian, K., Walsh, T. J., Capobianco, R., Devlic, A., Eckert, F., Fuchs, F., et al. (2022). Outracing champion Gran Turismo drivers with deep reinforcement learning. *Nature*, 602(7896):223–228.
- Xin, X., Tu, Y., Stojanovic, V., Wang, H., Shi, K., He, S., & Pan, T. (2022). Online reinforcement learning multiplayer non-zero sum games of continuous-time Markov jump linear systems. *Applied Mathematics and Computation*, 412:126537.
- Xu, X., Cai, P., Ahmed, Z., Yellapu, V. S., & Zhang, W. (2022a). Path planning and dynamic collision avoidance algorithm under COLREGs via deep reinforcement learning. *Neurocomputing*, 468:181–197.
- Xu, X., Lu, Y., Liu, G., Cai, P., & Zhang, W. (2022b). COLREGs-abiding hybrid collision avoidance algorithm based on deep reinforcement learning for USVs. *Ocean Engineering*, 247:110749.
- Xu, X., Lu, Y., Liu, X., & Zhang, W. (2020). Intelligent collision avoidance algorithms for USVs via deep reinforcement learning under COLREGs. *Ocean Engineering*, 217:107704.
- Yasukawa, H. & Yoshimura, Y. (2015). Introduction of MMG standard method for ship maneuvering predictions. *Journal of Marine Science and Technology*, 20(1):37–52.
- Zaccone, R., Martelli, M., & Figari, M. (2019). A COLREG-compliant ship collision avoidance algorithm. In *European Control Conference*, pages 2530–2535. IEEE.
- Zhai, P., Zhang, Y., & Shaobo, W. (2022). Intelligent ship collision avoidance algorithm based on DDQN with prioritized experience replay under COLREGs. *Journal of Marine Science and Engineering*, 10(5):585.
- Zhao, L. & Roh, M.-I. (2019). COLREGs-compliant multiship collision avoidance based on deep reinforcement learning. *Ocean Engineering*, 191:106436.
- Zhao, W., Queraltá, J. P., & Westerlund, T. (2020). Sim-to-real transfer in deep reinforcement learning for robotics: A survey. In *Symposium Series on Computational Intelligence*, pages 737–744. IEEE.

- Zhou, C., Wang, Y., Wang, L., & He, H. (2022). Obstacle avoidance strategy for an autonomous surface vessel based on modified deep deterministic policy gradient. *Ocean Engineering*, 243:110166.
- Zhou, X.-Y., Huang, J.-J., Wang, F.-W., Wu, Z.-L., & Liu, Z.-J. (2020). A study of the application barriers to the use of autonomous ships posed by the good seamanship requirement of COLREGs. *The Journal of Navigation*, 73(3):710–725.
- Zhou, Y., Daamen, W., Vellinga, T., & Hoogendoorn, S. (2019a). Review of maritime traffic models from vessel behavior modeling perspective. *Transportation Research Part C: Emerging Technologies*, 105:323–345.
- Zhou, Z., Kearnes, S., Li, L., Zare, R. N., & Riley, P. (2019b). Optimization of molecules via deep reinforcement learning. *Scientific Reports*, 9(1):1–10.

Appendix A. Selected COLREG rules

In the following, we present some of the rules from the International Maritime Organization (1972).

Rule 6: Safe speed

Every vessel shall at all times proceed at a safe speed so that she can take proper and effective action to avoid collision and be stopped within a distance appropriate to the prevailing circumstances and conditions.

Rule 7: Risk of collision

(a) Every vessel shall use all available means appropriate to the prevailing circumstances and conditions to determine if risk of collision exists. If there is any doubt such risk shall be deemed to exist.

Rule 8: Action to avoid collision

(a) Any action to avoid collision shall be taken in accordance with the Rules of this Part and shall, if the circumstances of the case admit, be positive, made in ample time and with due regard to the observance of good seamanship.

(b) Any alteration of course and/or speed to avoid collision shall, if the circumstances of the case admit, be large enough to be readily apparent to another vessel observing visually or by radar; a succession of small alterations of course and/or speed should be avoided.

(c) If there is sufficient sea-room, alteration of course alone may be the most effective action to avoid a close-quarters situation provided that it is made in good time, is substantial and does not result in another close-quarters situation.

(d) Action taken to avoid collision with another vessel shall be such as to result in passing at a safe distance. The effectiveness of the action shall be carefully checked until the other vessel is finally past and clear.

Rule 14: Head-on situation

(a) When two power-driven vessels are meeting on reciprocal or nearly reciprocal courses so as to involve risk of collision each shall alter her course

to starboard so that each shall pass on the port side of the other.

Rule 15: Crossing situation

When two power-driven vessels are crossing so as to involve risk of collision, the vessel which has the other on her own starboard side shall keep out of the way and shall, if the circumstances of the case admit, avoid crossing ahead of the other vessel.

Rule 16: Action by give-way vessel

Every vessel which is directed to keep out of the way of another vessel shall, so far as possible, take early and substantial action to keep well clear.

Appendix B. Hyperparameters of the baseline methods

In this section, we provide the hyperparameters of the baseline methods used in our experiments to ensure full reproducibility. We refer the reader to the respective papers for a detailed description of each method and the precise meaning of the parameters. Both methods generate output in the form of an OS heading, which we do not allow to deviate from the OS’s current heading by more than 2.5° . This is to prevent these methods from having a significant advantage over the DRL approach in terms of manoeuvrability.

The first baseline method is the APF approach proposed by Lyu and Yin (2019). To optimise the method’s hyperparameters for our validation scenarios, we performed a small grid search and set the emergency scaling factor for close-range obstacles, η_e , to 5,000 and the safe distance, d_{safe} , to 0.5 nautical miles. The remaining hyperparameters are the same as those used by Lyu and Yin (2019).

The second baseline method is the VO approach outlined by Kuwata et al. (2014). Due to the lack of values in their paper, we replaced their COLREG situation classification with the values given in Table 1 and optimised the remaining parameters via a small grid search. This resulted in the pre-collision check parameters being set to $t_{\text{max}} = 15$ minutes and $d_{\text{min}} = 0.75$ NM, and the hysteresis parameter was set to $n_h = 60$. Since our DRL agent and the APF method of Lyu and Yin (2019) only adjust the rudder angle and heading, respectively, we assume that the absolute value of the OS velocity is constant and only optimise for a heading angle in the VO method. At each step, we thus evaluate $N = 500$ equally spaced candidate headings over the interval $[\phi_{OS} - \frac{\pi}{2}, \phi_{OS} + \frac{\pi}{2}]$ and select the headings that are not in a VO-

or COLREG-constrained velocity set (see Kuwata et al. (2014)). We then select the heading that results in a velocity vector with a minimum 2-norm distance to the velocity vector towards the goal. This corresponds to setting the cost parameters of Kuwata et al. (2014) to $\omega_\tau = 0$ and $\omega_v = 1$, and the weighting matrix Q is the identity matrix.

Appendix C. Around the Clock: Distances

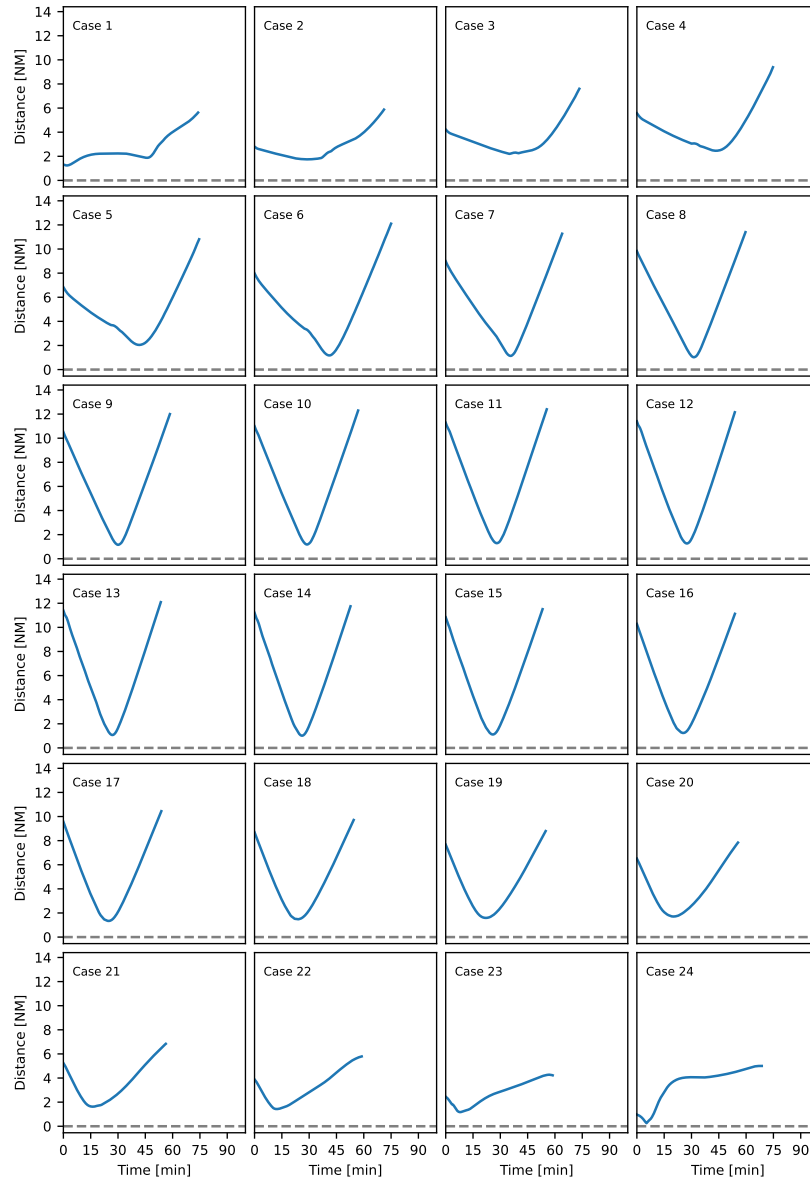


Figure C.1: Distances between the DRL agent and the target ship during the Around the Clock scenarios. Following our definition of a collision, a distance of zero does not equate to a physical collision; it indicates that the TS's midship position is exactly at the border of the agent's ship domain.

Appendix D. Imazu problem constellations

Case	Target Ship 1			Target Ship 2			Target Ship 3		
	ϕ [°]	N [NM]	E [NM]	ϕ [°]	N [NM]	E [NM]	ϕ [°]	N [NM]	E [NM]
1	180	6.009	0.000	-	-	-	-	-	-
2	-90	0.000	6.009	-	-	-	-	-	-
3	0	-2.337	0.000	-	-	-	-	-	-
4	45	-4.249	-4.249	-	-	-	-	-	-
5	180	6.009	0.000	-90	0.000	6.009	-	-	-
6	-10	-5.918	1.043	-45	-4.249	4.249	-	-	-
7	0	-2.337	0.000	-45	-4.249	4.249	-	-	-
8	180	6.009	0.000	-90	0.000	6.009	-	-	-
9	-30	-5.204	3.004	-90	0.000	6.009	-	-	-
10	-90	0.000	6.009	15	-5.804	-1.555	-	-	-
11	90	0.000	-6.009	-30	-5.204	3.004	-	-	-
12	180	6.009	0.000	-45	-4.249	4.249	-10	-5.918	1.043
13	180	6.009	0.000	10	-5.918	-1.043	45	-4.249	-4.249
14	-10	-5.918	1.043	-45	-4.249	4.249	-90	0.000	6.009
15	0	-2.337	0.000	-45	-4.249	4.249	-90	0.000	6.009
16	45	-4.249	-4.249	90	0.000	-6.009	-90	0.000	6.009
17	0	-2.337	0.000	10	-5.918	-1.043	-45	-4.249	4.249
18	-135	4.249	4.249	-15	-5.804	1.555	-30	-5.204	3.004
19	15	-5.804	-1.555	-15	-5.804	1.555	-135	4.249	4.249
20	0	-2.337	0.000	-15	-5.804	1.555	-90	0.000	6.009
21	-15	-5.804	1.555	15	-5.804	-1.555	-90	0.000	6.009
22	0	-2.337	0.000	-45	-4.249	4.249	-90	0.000	6.009

Table D.1: Starting positions of the target ships in the Imazu problems, with heading angles built on the work of Sawada et al. (2021) and Zhai et al. (2022).